Minerals Engineering 167 (2021) 106836

Contents lists available at ScienceDirect

Minerals Engineering

journal homepage: www.elsevier.com/locate/mineng

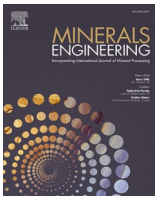

Uncertainties in quantitative mineralogical studies using scanning electron microscope-based image analysis

Rosie Blannin [a,*], Max Frenzel [a], Laura Tuşa [a], Sandra Birtel [a], Paul Ivăşcanu [b,1], Tim Baker [b], Jens Gutzmer [a]

[a] Helmholtz-Zentrum Dresden-Rossendorf, Helmholtz Institute Freiberg for Resource Technology, Freiberg, Germany
[b] Eldorado Gold Corporation, Vancouver, Canada

ARTICLE INFO

Keywords:
Geometallurgy
Automated mineralogy
Nugget effect
Uncertainty estimation
Bootstrap resampling

ABSTRACT

Scanning electron microscope-based automated mineralogy studies are readily associated with quantitative results, providing one of the foundations of geometallurgical studies. Despite the importance of quantitative data for such studies, and efforts to reduce statistical errors, the reporting of uncertainties is rare. This contribution illustrates how bootstrap resampling can be used to provide robust estimates of statistical uncertainties for the modal mineralogy, metal deportment and all relevant textural attributes of a sample or a series of samples. Based on a case study of the Bolcana Au-Cu porphyry deposit in the South Apuseni Mountains, Romania, the impact of insufficient sampling statistics on quantitative mineralogical studies is illustrated. Quantitative analyses of the mineralogy and microfabric of milled ore samples from seven 40 m drill core intervals from the Bolcana Prospect were conducted using a Mineral Liberation Analyser (MLA), complemented by electron probe micro-analysis. Bootstrap resampling was then applied to assess how many grain mount surfaces should be analysed to achieve statistically robust results for both Cu and Au mineralogy, deportment and textural attributes. Despite variable mineralogy, grades and mineralisation styles, estimated statistical uncertainties on Cu deportment are consistently low. In contrast, uncertainties for Au deportment are so high that most reported values for important characteristics are statistically meaningless. This is mainly attributed to the pronounced nugget effect for Au mineralisation, exacerbated by the small sample size analysed by MLA. An unfeasible number of measurements would be necessary to provide robust figures for the deportment of minor/trace elements and minerals, along with other tangible mineralogical properties, such as mineral associations. The results of this case study demonstrate that statistical uncertainties need to be carefully incorporated when considering the results of automated mineralogical studies and their impact on geometallurgical models. This is particularly relevant for studies of precious metal ores.

1. Introduction

Tangible ore characteristics, such as mineralogy, metal deportment and microfabric constrain the efficiency of mineral processing operations and, therefore, are important factors to consider during the exploration and evaluation stages of a mining project (Core et al., 2006; Cropp et al., 2013; Gregory et al., 2013; Kesler et al., 2002). Modern analytical techniques, such as scanning electron microscope-based automated mineralogy systems (e.g. Mineral Liberation Analyser, QEMSCAN, Mineralogic, TIMA-X), allow quantitative data on these characteristics to be acquired both quickly and relatively cheaply. Due to the wealth of information these techniques provide, they are commonly applied in geometallurgical studies (Bachmann et al., 2018; Frenzel et al., 2018; Kern et al., 2018; Leichliter, 2013). They are also frequently used to numerically constrain the deportment of rare and precious metals (e.g. Goodall, 2008; Goodall and Butcher, 2012; Gregory et al., 2013; Warlo et al., 2019; Zhou et al., 2009). However, such studies do not typically report any statistical errors and thus, the robustness of the results remains uncertain, as well as any technical decisions taken based on these results.

Several methods have been employed to estimate uncertainties on automated mineralogy-derived measurements. For example, Lastra and

* Corresponding author.
E-mail address: r.blannin@hzdr.de (R. Blannin).
[1] Present address Dundee Precious Metals, Sofia, Bulgaria

https://doi.org/10.1016/j.mineng.2021.106836
Received 11 September 2020; Received in revised form 9 February 2021; Accepted 11 February 2021

Paktunc (2016) investigated variability in mineral quantity and mineral liberation analyses through inter-laboratory testing of the +208 to -509 μm fraction of a sulphide flotation rougher concentrate. They found a good agreement in the mineral quantities, but less agreement in the liberation and mineral association analyses. Therefore, correct mineral quantities do not necessarily imply correct mineral liberation and association. In another approach, Benvie et al. (2013) developed a statistical approach for using automated mineralogy analyses in conjunction with diagnostic leaching tests. It was determined that measurements of at least two grain mounts were required for each head and leach residue sample, to derive the background variance and standard deviation. Butcher et al. (2000) analysed a sulphide flotation concentrate from KCGM's Super Pit operations in Kalgoorlie, Western Australia, using automated mineralogy to quantify gold deportment. Twenty polished blocks of the same sample were analysed, with an average of three gold grains identified per sample replicate. Analyses of 13 of these blocks were required for 90 % confidence of capturing the mean number of grains i.e. to produce statistically reliable results. More recently, Guseva et al. (2021) applied the point counting method with the binomial distribution approximation (Chayes, 1945; 1944; Guseva et al., 2021; Van der Plas and Tobi, 1965) to evaluate analytical errors on mineralogical measurements. The study suggested that the binomial distribution approximation may not be adequate in all cases, particularly for coarse materials, and that other methods should be applied in such cases, e.g. bootstrap resampling or the estimation of confidence intervals based on the method developed by Leigh et al. (1993).

Bootstrap resampling has been identified as an effective tool for the estimation of errors on textural characteristics measured by automated mineralogy (Evans and Napier-Munn, 2013; Mariano and Evans, 2015). For example, the bootstrap approach has been used to provide uncertainties on particle properties measured by automated mineralogy for the statistical modelling and simulation of mechanical separation processes (Hannula et al., 2018), the evaluation of magnetic separation efficiency (Buchmann et al., 2018; Leißner et al., 2016) and density separation processes (Schach et al., 2019).

Bootstrap resampling involves taking ***M*** random subsets of ***N*** samples from a population, and replacing the randomly selected samples to ensure that the entire population is available to be selected again (Chernick, 1999; Efron, 1979). This method has been found to agree with accepted statistical methods for assessing error in mineral grades using point counting on polished sections (Chayes, 1945; 1944; Guseva et al., 2021; Van der Plas and Tobi, 1965), whilst having the advantages of being assumption-free, rather than assuming a binomial distribution, and being applicable to a wide range of particle characteristics (Evans and Napier-Munn, 2013). Based on these methods, the standard deviation of mineral grades is proportional to the square root of the total area of the particles measured, or the number of particles measured. Following on from this, when comparing results from different methods (X-ray powder diffraction, automated mineralogy, element to mineral conversion), Parian et al. (2015) estimated the relative standard deviation of measurements for any mineral grade using:

$$RSD = ax^{-0.5} \quad (1)$$

where x is the mineral grade, RSD is the relative standard deviation and a is a coefficient, which implies that relative standard deviation is proportional to the square root of the mineral grade.

The bootstrap method can also be used to determine how many grains (i.e. total area) need to be measured in order to reach a given uncertainty (Evans and Napier-Munn, 2013; Mariano and Evans, 2015). Evans and Napier-Munn (2013) determined that measurements of only two polished block surfaces are required to achieve a Relative Standard Deviation (*RSD*) of 10 % for chalcopyrite grade in samples from a porphyry Cu deposit. In contrast, around 16 blocks would need to be measured to achieve the same *RSD* for the chalcopyrite grain size distribution, similar to the finding of Lastra and Paktunc (2016), due to the high uncertainties associated with the coarse size fractions.

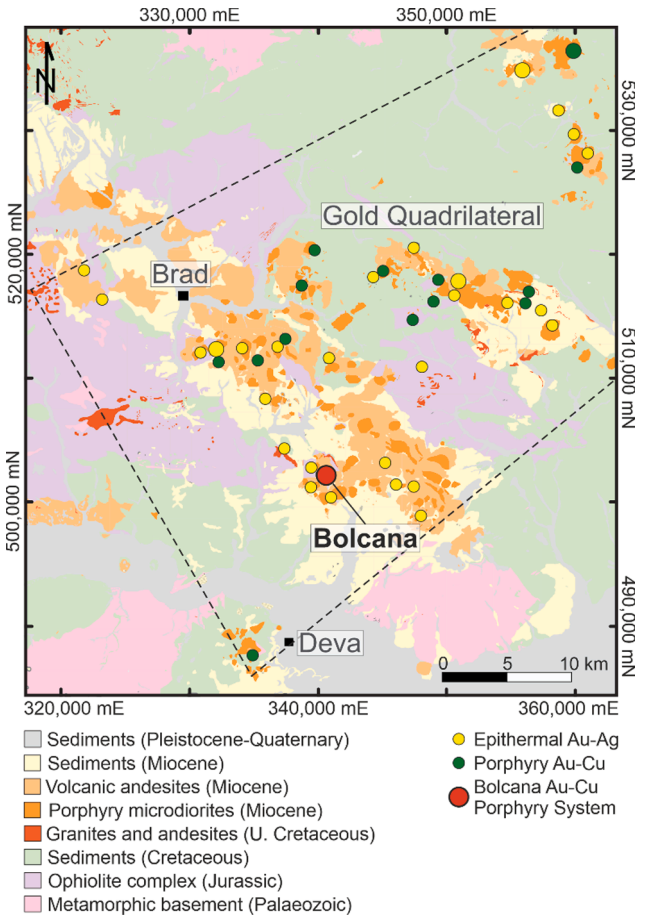

Fig. 1. Simplified geological map of the "Gold Quadrilateral", South Apuseni Mountains. Epithermal Au-Ag and porphyry Cu-Au systems are highlighted. Modified after Ivăşcanu et al. (2018).

Despite bootstrap resampling being a well-documented and proven approach for the estimation of uncertainties for automated mineralogy data, statistical uncertainties are rarely reported. Such uncertainties are particularly important for process mineralogical and geometallurgical studies of precious metal ores, as these are typically marked by extremely low (mineral) grades. Without the reporting of uncertainties, it cannot be assumed that enough precious mineral grains have been analysed to ensure reliable data and robust statistics. Therefore, the quantitative nature of such studies must be questioned.

This study demonstrates how the errors associated with automated mineralogical studies can be estimated and reported, using the bootstrap technique, to ensure that technical decisions take uncertainty of the results into account. The Bolcana porphyry Au-Cu system in Romania was used as a case study. As an early stage exploration project, Bolcana provides an ideal environment for a geometallurgical assessment. Automated mineralogy was applied, in combination with complementary analytical techniques, to characterise samples from a series of metallurgical testing intervals, focused mainly on copper and gold deportment, as well as mineral associations. The implications of the findings are assessed and recommendations provided for future process mineralogical studies in terms of sampling strategy, analytical work and reporting of statistical uncertainties.

2. Case study

The Bolcana porphyry gold-copper system is located in the Western Tethyan magmatic belt, where the tectonic and geodynamic setting evolved from Cretaceous subduction-related arc magmatism,

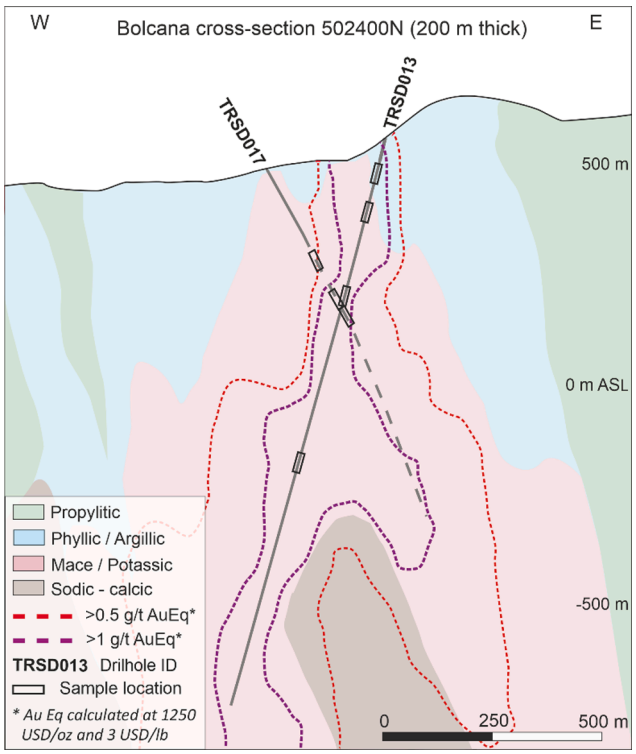

Fig. 2. Schematic cross section, derived from a 3D model, through the Bolcana porphyry system, showing principal alteration domains gold. Gold-equivalent grade shells of > 0.4 g/t (red) and > 1.0 g/t (purple) were calculated using prices of 1,250 USD/oz Au and 3 USD/lb Cu. The studied drill holes, TRDS017 and TRSD013, are shown, with the studied intervals also highlighted for TRSD013.

transitioning from convergence to post-orogenic extension in the late Eocene to early Oligocene, followed by widespread post-collisional extension-related magmatism in the Miocene (Baker, 2019). The Bolcana deposit can be further localised to the Brad-Sacaramb metallogenic district within the "Gold Quadrilateral" of the South Apuseni Mountains, Romania, where the metallogenic endowment is related to Miocene magmatism (Fig. 1). In comparison to the rest of the West Tethyan belt, this region hosts significant Au resources, forming Europe's largest epithermal Au-Ag-Te province. With twenty known porphyry copper deposits, it is also one of Europe's most important porphyry Cu-Au provinces (e.g. Baker, 2019; Berbeleac et al., 2014; Cioacă, 2013; Milu et al., 2003).

The porphyry mineralisation of the Bolcana system is being explored by Eldorado Gold Corporation through its Romanian subsidiary, Deva Gold S.A., who recently published a maiden resource estimate of 381 Mt at 0.53 g/t gold and 0.18 % copper (Ivăşcanu et al., 2019, 2018). The Bolcana system comprises a sequence of complex cross-cutting porphyry phases, breccias, alteration and veining. Early-stage crowded diorite porphyries host copper–gold mineralisation and exhibit a classical evolution of vein density and mineralisation decreasing from early to intra to late mineral phases (Sillitoe, 2010), with potassic (biotite-feldspar-magnetite) and sodic (albite-actinolite-epidote-chlorite-magnetite) alteration. Extensive phreatomagmatic brecciation developed in the roof of the crowded porphyry system, which were subsequently intruded by fine, uncrowded andesitic to microdioritic intermineral porphyry dykes and breccias. Alteration of these fine intermineral porphyries is dominantly potassic with a strong and pervasive magnetite-albite-chlorite-epidote (MACE) overprint. The fine intermineral porphyries, magmatic breccias and magmatic-hydrothermal breccias have higher gold grades, but typically lower copper grades, than the earlier crowded porphyries (Ivăşcanu et al., 2019, 2018). In the periphery of the deposit, porphyry mineralisation is accompanied by Pb-ZnCuAuAg intermediate-sulphidation epithermal veins (Cardon et al., 2008; Ivăşcanu et al., 2018).

3. Materials and methods

3.1. Sampling and sample preparation

Seven drill core intervals, each 40 m in length, from two drill holes were selected for this study: TRSD017 240–280 m, 346–386 m and 386–26 m; TRSD013 64–104 m, 152–192 m, 356–396 m and 758–798 m; as shown in the simplified cross section in Fig. 2. Details on the lithology, alteration, mineralisation, and location of the drill core intervals within the deposit are provided in Table 1.

Representative splits, around 100 g, of crushed (~ 2 mm) drill core material were provided by Deva Gold S.A for every 2 m section of the studied testing intervals. Representative samples of the 40 m intervals were constituted by mixing representative splits (25 g) of the respective sub-samples for each interval, homogenising and milling to a 100 % pass size of 600 µm in a Laarmann LMBM 2000 planetary mill at 200 revolutions per minute (rpm), and with steel balls of 20 mm diameter. For interval TRSD013 152–192 m, additional 4 m interval samples were prepared to enable a more detailed assessment of the variable and relatively high gold content detected in this interval. The samples were prepared in the same way, by splitting and homogenisation, and then milled in a Retsch RS 200 disc mill at 700 rpm. All 17 samples were then split again to around 4 g (7 samples from 40 m intervals, 10 samples from 4 m intervals of TRSD013 152–192 m). Sample preparation was performed at the Helmholtz Institute Freiberg for Resource Technology (HIF).

Table 1
Information on selected drill core intervals. Alteration types: Po = Potassic, So = Sodic, MACE = Magnetite-albite-chlorite-epidote.

Drill hole ID	From-To (m)	Zone	Lithology	Alteration	Mineralisation
TRSD013	64–104	Shallow, central	Intermineral porphyry ± breccia	Moderate Po/So/MACE, moderate/strong clay overprint	Ccp-Py, Cv-Cct replacement
	152–192	Shallow, high grade, central	Fine grained porphyry	Strong Po/So, moderate clay overprint	Ccp, Py, Bn, Cv-Cct replacement
	356–396	Intermediate, central	Breccia, porphyry dykes/ veins	Strong Po/So, moderate clay alteration on veins	Ccp and Py
	758–798	Deep, high grade, West	Fine grained porphyry	Strong Po/So	Ccp and Bn, low py
TRSD017	240–280	Shallow, low grade, South	Breccia, porphyry dykes/ veins	Po/So/MACE, variable clay overprint	Ccp, Py, local base metals
	346–386	Moderate grade, South	Intermineral porphyry ± breccia	Po/So/MACE, weak clay overprint	Ccp, Py
	386–426	High grade, South	Fine grained porphyry	Po/So/MACE, weak clay overprint	Ccp, Py, Bn

Table 2
SEM and MLA operating conditions (Acc. volt. = acceleration voltage; Probe cur. = probe current; BSE cal. = Back Scatter Electron calibration; Res. = resolution; pix. = pixels; Acq. time = acquisition time; Min. part. size = minimum particle size).

SEM settings	GXMAP	SPL-DZ	MLA settings	GXMAP	SPL-DZ
Acc. volt. (kV)	25		Pixel size (μm)	1.5	0.625
Probe cur. (nA)	10		Res. (pix.)	1000 × 1000	
Spot size	5.6		Step size (pix.)	6 × 6	
HFW	1500	1000	Acq. time (ms)	55	
Brightness	96.2		BSE trigger	26–255	225–255
Contrast	18.5		Min. part.. size (pix.)	5	1
BSE cal. (Au)	254		Min. grain size (pix.)	3	1

3.2. Chemical assays

Chemical assays were carried out by ALS Romania SRL for a total of 49 elements on every 2 m interval of drill core (140 samples). The assaying procedure involved four acid digestion followed by inductively coupled plasma mass spectrometry (ICP-MS) for all elements, with the exception of Au, which was analysed by fire assay with an atomic absorption spectroscopy finish. The results were provided by Deva Gold S. A. and were used to check the validity of the mineralogical studies.

3.3. Mineral liberation Analyser

An MLA instrument was used to analyse the samples and provide quantitative mineralogical and microstructural data (Fandrich et al., 2007; Gu, 2003; Schulz et al., 2020). Polished grain mounts (30 mm) of the milled samples (pass size of 600 μm) were prepared by mixing the sample with pure graphite powder and embedding the mixture in epoxy resin. The initial sample blocks were sliced vertically, rotated by 90° and remounted in epoxy resin before polishing, to reduce the effects of gravity settling (Heinig et al., 2015). The polished grain mounts were carbon coated in preparation for MLA. To improve measurement statistics, the grain mounts of the 40 m blend samples were re-ground and polished, and the MLA analyses repeated, with a total of six surfaces measured for each 40 m sample. Therefore a total of 52 analyses were performed: 6 analyses for each 40 m samples (42) and one analysis for each 4 m sample from interval TRSD013 152–192 m (10).

Analyses were performed at HIF on an FEI Quanta 650F field emission SEM (FE-SEM) equipped with two Bruker Quantax X-Flash 5030 energy-dispersive X-ray (EDX) detectors and the MLA software suite version 3.0. The GXMAP and SPL-DZ measurement modes were used, with details of the modes found in Fandrich et al. (2007). The operating conditions used for SEM and MLA are listed in Table 2.

The complex and fine-grained nature of the samples led to the generation of mixed spectra during MLA measurements, and the misclassification of fine gold grains. To remedy this, manually created mixed spectra (cf. Bachmann et al. (2017); Kern et al. (2018) for this approach). between gold and common host minerals (chalcopyrite, pyrite and quartz) were added to the mineral reference list at ratios of 50:50, 60:40, 70:30, 80:20 and 90:100 (Au:Mineral). To prevent over-estimation of copper and gold grades using MLA, Back Scatter Electron (BSE) Overlay scripts were applied to remove pixels with BSE levels lower than 190 for gold, 170 for the gold mixed spectra and 92 for chalcopyrite. Spectra matching was set at 90 % for the GXMAP measurements, and 80 % for the SPL measurements.

3.4. Electron probe microanalysis

Four crushed material samples were selected for electron probe microanalysis (EPMA) to identify any sulphides that carry significant gold content. The TRSD013 64–104 m, TRSD017 386–426 m and TRSD013 758–798 m samples were chosen to represent shallow, moderate and high depths of the deposit. TRSD013 184–188 m was selected based on the high Au content as reported by the chemical assay. See Appendix A.1 for more information on the EPMA methodology, with the detailed measurement settings in Table A1.

3.5. Estimation of analytical uncertainties

Uncertainties of MLA-derived data were estimated using the bootstrap resampling method (Chernick, 1999; Efron, 1979), including calculated assays of copper and gold, modal mineralogy, copper deportment, grain size and mineral associations of relevant ore minerals of copper and gold. Bootstrap resampling is an effective technique for the estimation of errors associated with quantitative automated mineralogy-derived measurements of the textural characteristics of particulate materials (Evans and Napier-Munn, 2013; Mariano and

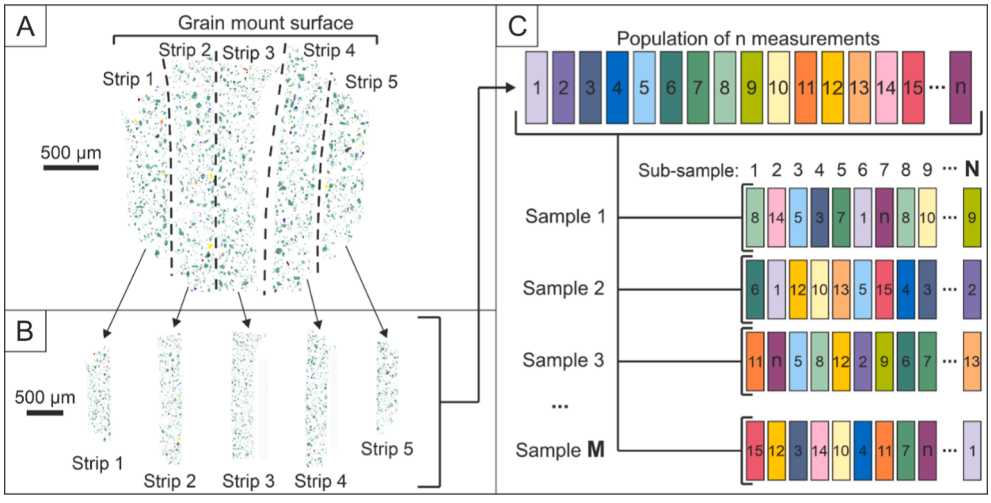

Fig. 3. Schematic diagram to illustrate: (A) an MLA false colour image of a whole grain mount surface; (B) how each grain mount surface was split into 5 strips; (C) the process of bootstrap resampling to sample ***M*** sets of ***N*** sub-samples from an original population of *n* samples.

Evans, 2015). The bootstrap resampling method involves creating $\boldsymbol{M}$ subsets of $\boldsymbol{N}$ samples, by randomly sampling the original sample set. Using replacement, every sample from the original population is available for selection each time. A schematic diagram is provided in Fig. 3.C, where n strips are available in the original population, and $\boldsymbol{M}$ samples are constituted by taking $\boldsymbol{N}$ random samples.

In this study, composite ground material samples from seven 40 m intervals were analysed with MLA. After repeated re-grinding and re-polishing, six surfaces were measured for every grain mount, each comprising 5 strips, resulting from the rotation of the original grain mounts (see details in Section 3.4; Fig. 3.A-B). The bootstrap resampling was performed by sampling and replacing from the total of 30 strips (5 strips in each of the 6 measured surfaces) for which data were obtained. To estimate the errors on the textural characteristics of the particulate samples, $\boldsymbol{N}$ was set as the number of strips (i.e. 30) and 1000 subsets of $\boldsymbol{N}$ strips were randomly selected from the original set of 30 strips (i.e. $\boldsymbol{M} = 1000$). For the 4 m interval samples from interval TRSD013 152–192 m, only one grain mount surface was measured and so 5 strips were available, and therefore $\boldsymbol{N}$ was 5 for these samples.

The area of each mineral group in the resampled strips was summed and the overall modal mineralogy, copper and gold contents, and copper deportment were calculated using the mineral densities and stoichiometric mineral compositions. Mineral associations for chalcopyrite were calculated by dividing the summed contact lengths of chalcopyrite with each mineral by the total length of the chalcopyrite grain boundaries (Fandrich et al., 2007; Gu, 2003), according to the formula:

$$Mineral\ association = X/Y \tag{2}$$

where X is the length of grain boundaries between two specific minerals and Y is the total length of the grain boundaries of one of the minerals. The MAMA ratio (cf. Kern et al., 2019) was subsequently calculated to identify preferential associations using the following formula:

$$MAMA = \frac{Mineral\ \ Association\ \ of\ \ target\ \ mineral\ \ with\ \ Min_X}{Mineral\ \ Area\ \ (\%)\ \ of\ \ Min_X} \tag{3}$$

where mineral association is calculated as given in equation (2), when free perimeter is excluded, and mineral area is the area percent of the associated mineral in the sample.

The mineral associations of gold were also investigated for intervals with >10 gold grains (TRSD013 64–104 m, 758–798 m and TRSD017 386–426 m), to ensure reliable sample statistics. Due to the low number of gold grains identified in each strip, bootstrap resampling of the gold mineral associations was performed on individual grains rather than using the strips. In this case, $\boldsymbol{N}$ was the number of gold grains present and $\boldsymbol{M}$ remained 1000. For interval TRSD013 152–192 m, the gold grains from both the 40 m and 4 m samples were combined and the associations were bootstrapped for the whole 40 m interval. A 'composite' of the gold grains from the 40 m samples was bootstrap resampled to provide an overview of gold mineral associations throughout all of the intervals. The gold grains from the 4 m samples from TRSD013 152–192 m were excluded to prevent over-representation of this interval.

Following the estimation of errors on the measurements, bootstrap resampling was applied to estimate how many grain mount surfaces would need to be measured for an acceptable relative standard deviation (see Section 5.1 for specific choices). *RSD*, also known as the coefficient of variation, is calculated as follows:

$$RSD = 100 \times \frac{\sigma}{\mu} \tag{4}$$

where σ is standard deviation and μ is the mean. $\boldsymbol{N}$ was increased in increments of 5, to represent a whole grain mount surface, until the required *RSD* was reached. The mineral association of gold was bootstrap resampled for the composite of the gold grains from the 40 m samples only, using individual grains rather than strips.

Table 3
The list of minerals identified by MLA with mineral groupings and abbreviations used for simplification purposes. The abbreviations are used in all following tables and figures.

	Group	Minerals	Abbreviation[4]
Rock-forming minerals	Quartz	Quartz	Qz
	Feldspars	K-feldspar, albite, labradorite	Fsp
	Amphiboles (+Pyroxene)	Hornblende, actinolite, wollastonite	Amp
Alteration minerals	White micas	Muscovite, illite	Wm
	Clay minerals	Kaolinite	Cly
	Biotite	Biotite	Bt
	Chlorite	Chamosite, clinochlore, other intermediate compositions	Chl
	Fe-oxides	Magnetite/hematite[1], titanomagnetite	Fe-O
	Carbonates	Calcite, siderite, ankerite	Cb
	Other alteration minerals	Epidote, allanite, gypsum/anhydrite[1], barite, fluorite	OAM
Cu-bearing minerals	Chalcopyrite	Chalcopyrite	Ccp
	Bornite	Bornite	Bn
	Chalcocite	Chalcocite	Cct
	Covellite	Covellite	Cv
	Sulphosalts	Tetrahedrite, freibergite	Ss
Sulphides	Pyrite	Pyrite	Py
	Other sulphide minerals	Sphalerite, galena, arsensopyrite, tellurobismuthite-pyrite[2]	OSM
Trace/minor minerals	Other minerals	Titanite, rutile, apatite, monazite, zircon	OM
Gold	Gold	Gold < 20 % Ag, Gold < 10 % Ag, Gold, Gold mixed spectra[3]	Gold

[1] Minerals cannot be distinguished by MLA.
[2] A mixed-spectra between tellurobismuthite and pyrite.
[3] Mixed spectra of gold and quartz, pyrite and chalcopyrite, as explained in Section 3.4.
[4] Mineral abbreviations according to Whitney and Evans (2010).

4. Results

The following subsections present the analytical results obtained by MLA, in combination with EPMA. The mineralogical variability, Cu and Au deportment, and mineral associations of chalcopyrite and gold grains of the samples are subsequently assessed, including estimations of the uncertainties related to the MLA measurements.

4.1. Mineralogical variability

A total of 44 minerals were identified in the samples using MLA. Further, the 44 phases were divided into 19 mineral groups as shown in Table 3. Note that feldspars and pyroxenes may well be both rock-forming and alteration minerals, but were grouped as rock-forming minerals for simplification. The area of each mineral was bootstrapped for each sample, as detailed in Section 3.5, and the modal mineralogy, with corresponding uncertainties, was subsequently calculated. The median simulated modal mineralogies are plotted in Fig. 4 for both the 40 m samples and the 4 m samples.

The contents of both the rock-forming (quartz, feldspars, amphiboles) and alteration minerals (white micas, clay minerals, chlorite, magnetite etc.) follow the well-established patterns of hydrothermal alteration and lithological transitions with depth in the Bolcana porphyry system (Dénes et al., 2015; Ivăşcanu et al., 2018; Ivăşcanu et al., 2019). Quartz content varies from ~ 15–35 wt%, in contrast to feldspars which increase from 10 wt% in the near-surface to around 50 wt% at the centre of the system. Amphiboles are typically a minor constituent.

Clay minerals and white micas are dominant in the near-surface, at

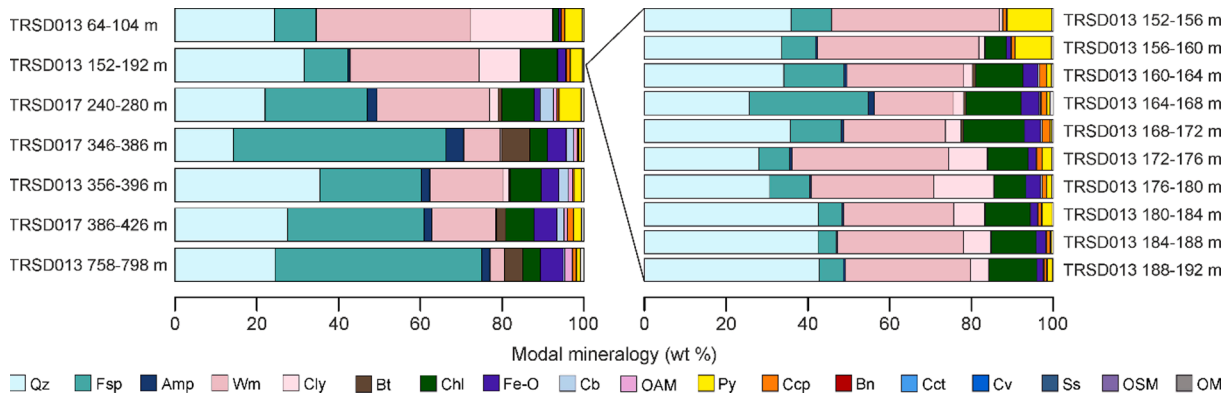

Fig. 4. Median modal mineralogy of the studied drill core intervals, from MLA GXMAP analyses of the 40 m crushed material samples (left) and the 4 m crushed material samples from drill hole interval TRSD013 152–192 m (right).

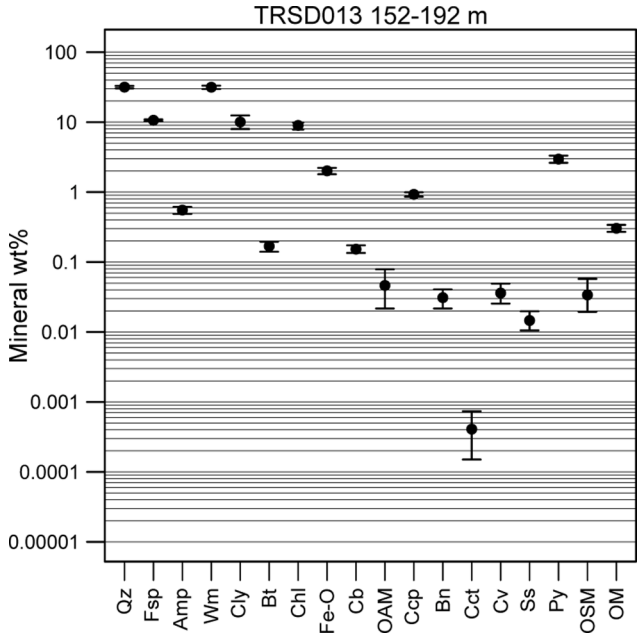

Fig. 5. Median value of bootstrapped modal mineralogy of sample TRSD013 152–192 m, with error bars plotted at the 2.5th and 97.5th percentiles to represent 95 % confidence intervals.

around 20 wt% and 38 wt% in TRSD013 64–104 m, respectively, in relation to phyllic alteration. Biotite content is linked to sodic and potassic alteration, occurring variably in the deeper intervals, up to around 7 wt% in TRSD017 346–386 m. Chlorite content is particularly associated with MACE (magnetite-albite-chlorite-epidote) alteration (Ivăşcanu et al., 2019, 2018), remaining fairly constant at higher depths (4–9 wt%). Fe-oxide content increases towards the centre of the system with the transition from sodic and MACE alteration assemblages towards the potassic core, reaching concentrations up to around 6 wt%. Other alteration minerals are typically minor in abundance.

Pyrite content is most significant in the phyllic alteration zone in the near-surface environment, at ~ 3–5 wt%. Chalcopyrite varies from ~ 0.3–1.5 wt%, with no clear trend with depth. Bornite, covellite, chalcocite, sulphosalts, sphalerite and galena are typically minor, at < 0.1 wt %, and also show no clear trend with depth. The lack of clear zoning in the sulphides results from variable lithology and alteration styles, combined with the complex architecture of cross-cutting porphyry bodies e.g. fine intermineral porphyries are dominantly associated with finely disseminated sulphides and/or C veins (chalcopyrite ± bornite ± pyrite), whereas strong potassic alteration is coincident with B veins hosting chalcopyrite (Ivăşcanu et al., 2019).

In the individual 4 m samples from the TRSD013 152–192 m interval, feldspar, clay, chlorite and pyrite contents vary considerably, while chalcopyrite content reaches around 2 wt%. The TRSD013 152–156 m interval is markedly different due to the high pyrite content (~ 11 wt%) and absence of chlorite. The pyrite content is similarly high in TRSD013 156–160 m (~ 9 wt%) and then decreases to < 2.5 wt% for the rest of the interval.

To assess the uncertainties of the modal mineralogy measurements, the median modal abundance values for different minerals were plotted

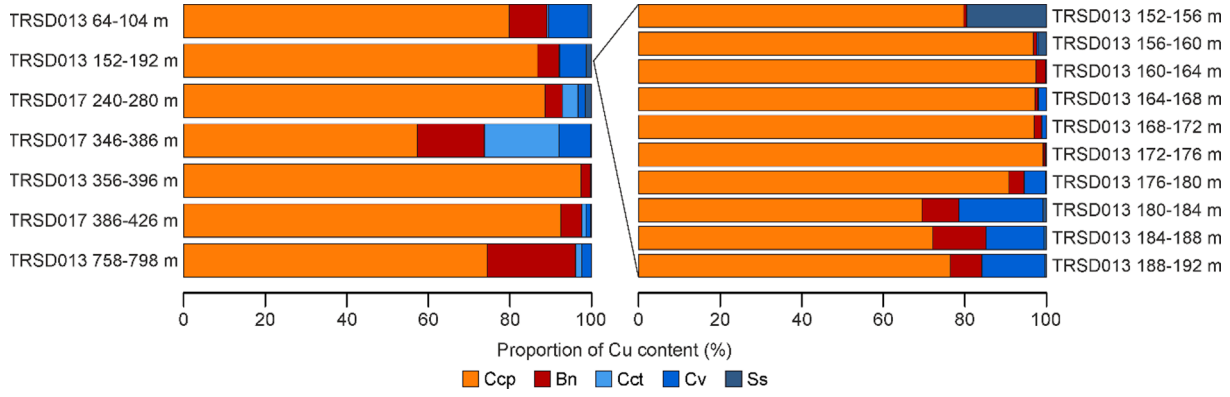

Fig. 6. Distribution of copper between Cu-bearing minerals in the 40 m crushed material samples (left) and the 4 m crushed material samples from drill hole interval TRSD013 152–192 m (right), calculated based on the median modal mineralogy from bootstrap resampling (Fig. 4).

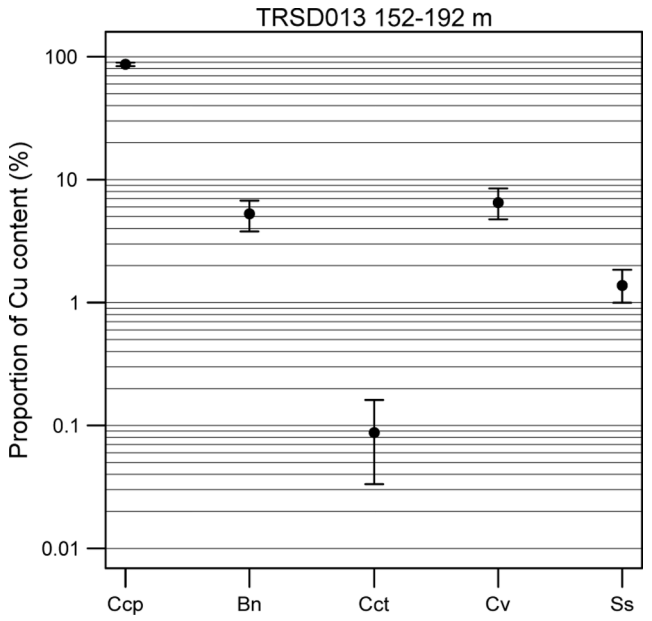

Fig. 7. Median value of boot strapped copper deportment of sample TRSD013 152–192 m, with 95 % confidence intervals.

with error bars representing 95 % confidence intervals. A graph for sample TRSD013 152–192 m is given in Fig. 5, as an example, with graphs for the remaining 40 m and 4 m intervals provided in Appendix B (Figs. B1 and B2). Uncertainties for the abundances of the major minerals in the 40 m samples tend to be low, typically with an *RSD* of < 10 %. For minerals with a modal content of around 0.1 wt% or less, the *RSD* increases above 10 %. Despite its relatively low content, the *RSD* of chalcopyrite is below 8 % in all 40 m samples. The highest *RSDs* are seen for minor Cu-bearing minerals, such as bornite (5–31 %), covellite (9–25 %), sulphosalts (13–47 %) and particularly chalcocite (19–100 %) and other sulphide minerals (9–39 %). High *RSDs* are also recorded for alteration minerals, which occur variably throughout the intervals, including clay minerals (4–47 %) and other alteration minerals (2–31 %). The uncertainties for mineral contents in the 4 m samples are rather high and variable. Only for quartz, feldspars, amphiboles and white micas are the *RSDs* below 10 % for each 4 m interval. Chalcopyrite has an *RSD* below 11 % in all samples.

4.2. Copper deportment

A combination of MLA and EPMA was used to study copper deportment in the Bolcana porphyry system. The copper deportment was calculated from the bootstrap resampling of the grain areas using the densities and mineral formulae provided by the standard MLA mineral reference lists. EPMA analyses of Cu sulphide mineral grains confirmed the general formulae used for the deportment calculations (Appendix A.2).

The median calculated copper deportments (Fig. 6) indicate that copper is hosted, rather variably, by chalcopyrite, bornite, chalcocite, covellite and the sulphosalts tetrahedrite and freibergite. Chalcopyrite is the most important Cu ore mineral in all samples, with between ~ 60–98 % of the overall Cu grade. The remaining Cu content is mainly hosted in bornite (~ 2–22 % of Cu grade), and variably contributed by chalcocite, covellite and sulphosalts. For instance, chalcocite is only significant in interval TRSD017 346–386 m (~ 16 %), while covellite contributes up to ~ 7 %. In the TRSD013 152–192 m interval 4 m samples, chalcopyrite remains the dominant Cu-bearing mineral, but sulphosalts (TRSD013 152–160 m), as well as bornite and covellite (TRSD013 180–192 m) contribute significantly to Cu-grade in some samples. The average measured areas of each Cu-bearing minerals are reported in Table A3, clearly showing again that chalcopyrite is the dominant Cu-bearing mineral in all samples by one or two orders of magnitude.

As could be expected, the uncertainties for Cu deportment are closely related to the uncertainties for the Cu-bearing mineral contents (Figs. 7, B.3 and B.4). The *RSDs* for chalcopyrite (< 7 %) and bornite (5–30 %) are typically low, being the most abundant Cu-bearing minerals. Conversely, chalcocite, covellite and sulphosalts contents are highly variable and therefore the uncertainties of their contributions to the Cu deportment are typically high, with *RSDs* from 19 to 102 % for chalcocite, 9–26 % for covellite and 11–46 % for sulphosalts. In the 4 m samples from TRSD013 152–192 m, the *RSDs* of chalcopyrite are lower than in the 40 m samples (0.1–5 %), while the other Cu-bearing minerals are similarly variable, or higher in the case of bornite (*RSDs* of 7–55 %).

4.3. Chalcopyrite mineral associations

The mineral associations of chalcopyrite, as the most important Cu-bearing mineral, were bootstrap resampled, based on the contact lengths of chalcopyrite grains with other minerals (Fig. 8). The dominant mineral associations reflect the modal mineralogy of the samples, with high association with the rock-forming and alteration minerals. The proportion of chalcopyrite potentially recoverable by froth flotation, i.e. with high free perimeter and association with sulphide minerals, is much higher than that associated with rock-forming and alteration minerals. However, the mineral associations do not provide information on the actual liberation of the chalcopyrite grains, and the free perimeter values should be treated with care, because the milling of the samples was performed under laboratory conditions which do not necessarily

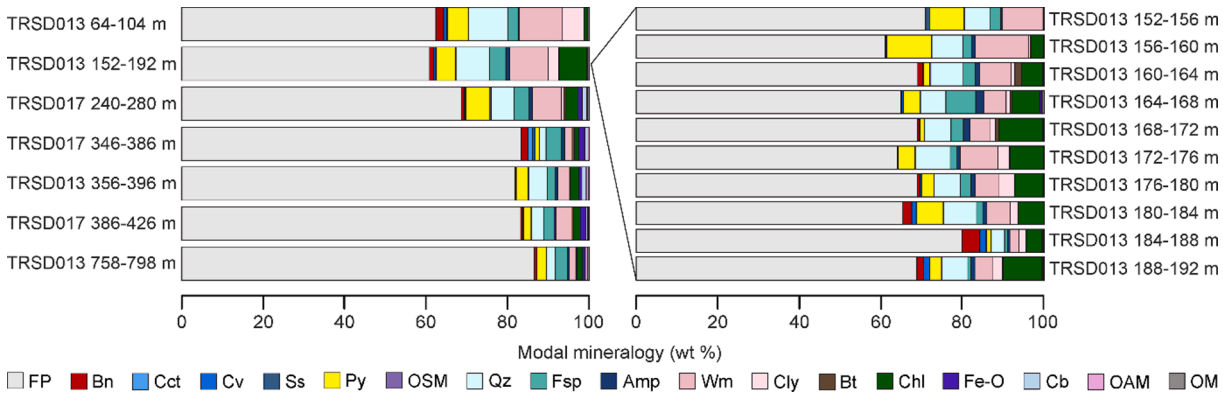

Fig. 8. Median bootstrapped chalcopyrite mineral associations (percentage of chalcopyrite grain perimeters) of the studied drill core intervals, from MLA GXMAP analyses of the 40 m crushed material samples (left) and the 4 m crushed material samples from drill hole interval TRSD013 152–192 m (right). FP = free perimeter, as also seen in some subsequent figures.

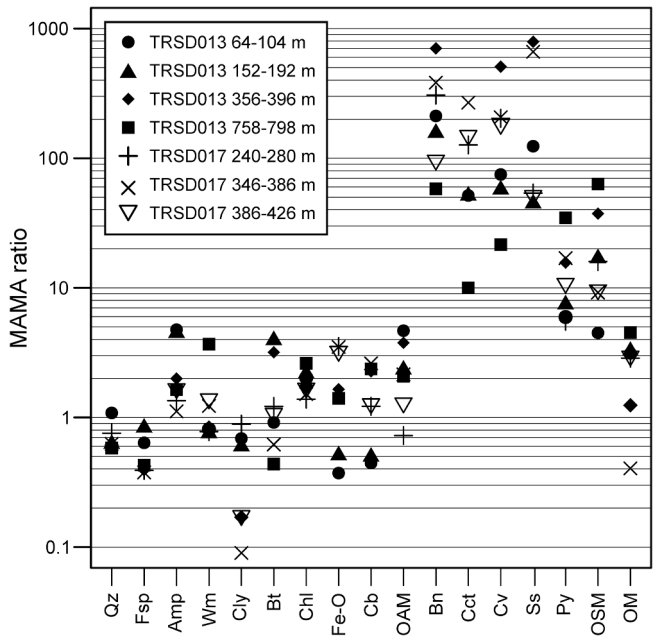

Fig. 9. Median MAMA ratio values of chalcopyrite for the 40 m interval samples, calculated from the bootstrap resampling results of chalcopyrite mineral associations and modal mineralogy.

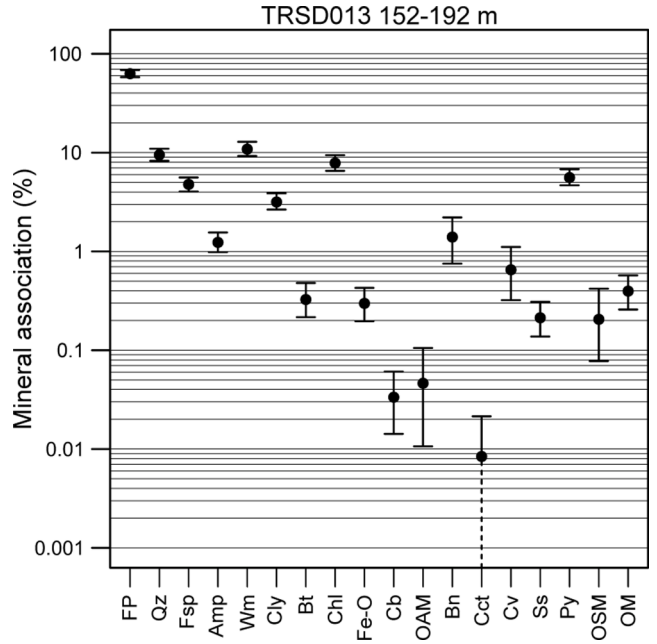

Fig. 10. Median value of bootstrapped chalcopyrite mineral associations (percentage of chalcopyrite grain perimeters) for TRSD013 152–192 m, with 95 % confidence intervals. The dashed line for chalcocite symbolises that the 2.5th percentile was 0, as also seen in some following figures.

correspond with industrial conditions.

The MAMA ratio was calculated to identify preferential associations, as seen for the 40 m intervals in Fig. 9 and the 4 m samples in Fig. B.5. There is a clear preferential association of chalcopyrite with other Cu-bearing minerals, with MAMA ratio values mostly exceeding 10 and reaching up to 800 for the 40 m samples (Fig. 9). Pyrite and other sulphide minerals have lower MAMA ratios, between 6 and 35 and 4–63, respectively, but the preferential association remains clear when compared to the rock-forming and alteration minerals which have

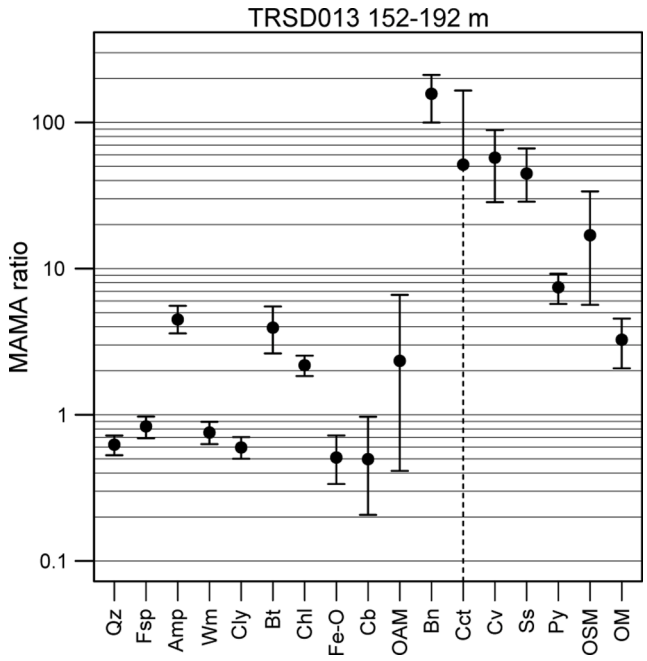

Fig. 11. Median value of MAMA ratio of chalcopyrite, calculated from the bootstrap resampling results of chalcopyrite mineral associations and modal mineralogy, for TRSD013 152–192 m, with 95 % confidence intervals.

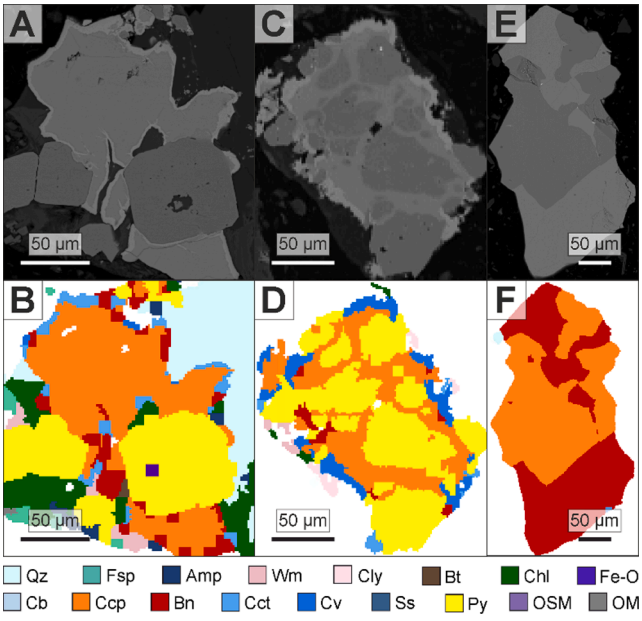

Fig. 12. BSE images (A,C,E) and false colour images from MLA (B,D,F) showing the preferential associations of Cu-bearing minerals and pyrite, from ground material samples TRSD017 240–280 m (A,B), TRSD013 164–168 m (C,D) and TRSD013 758–798 m (E,F). Chalcopyrite and pyrite are commonly intergrown (A–D) while rims of bornite, covellite and chalcocite form around chalcopyrite grains (A–D). Hypogene bornite occurring at greater depths is often associated with chalcopyrite (E,F).

maximum MAMA ratios of 5.

Overall, the mineral association uncertainties are high for all samples, with *RSD*s usually exceeding 10 % for most minerals (Figs. 10, 11, B.6). As could be expected, the uncertainties are lower for abundant minerals or those with a close association to chalcopyrite, including the main rock-forming and alteration minerals, and greater for those with lower abundances and/or lower preferential association. Although the

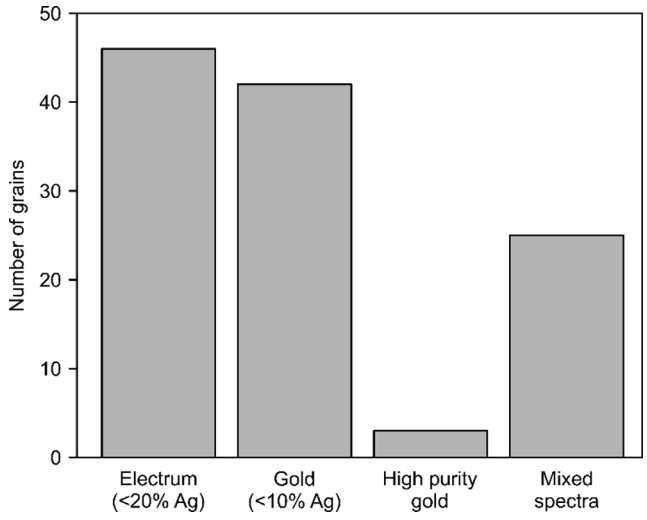

Fig. 13. Histogram of gold compositions for all gold grains identified in the studied samples.

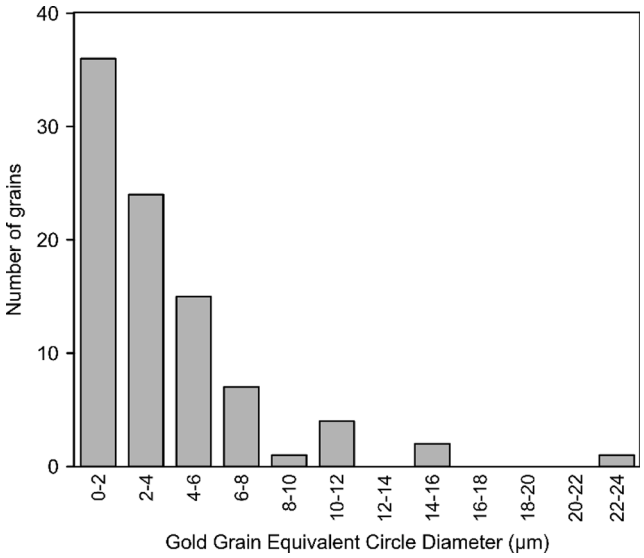

Fig. 14. Gold grain size distribution of all gold grains in the 40 m interval samples. The number of grains counted in each size fraction is given, based on the ECD of the grains measured by MLA.

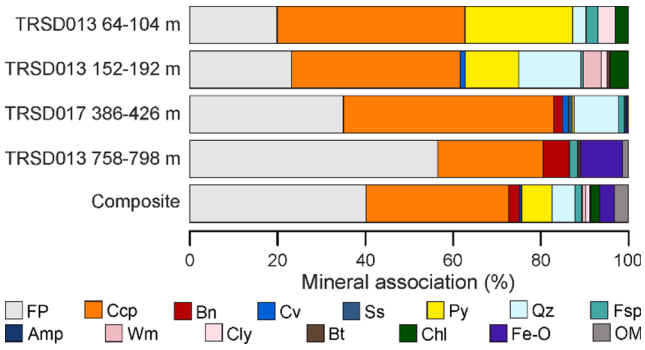

Fig. 15. Median bootstrapped gold mineral associations (percentage of gold grain perimeters) of the studied drill core intervals with > 10 gold grains. For interval TRSD013 152–192 m, the gold grains from both the 40 m and 4 m samples are included. The overall mineral associations for all gold grains are shown in the composite bar, including all grains from the 40 m crushed material samples.

association with bornite is rather variable (*RSDs* from 12 to 35 %), associations with the other Cu-bearing minerals are far more variable, with *RSDs* from 25 to 94 % for chalcocite, 13–71 % for covellite and 22–63 % for sulphosalts. The *RSDs* for the 4 m interval samples (Fig. B.7) are much higher than for the 40 m samples, with few values below 10 %. As could be expected, the *RSDs* on the MAMA ratio values are virtually the same as the equivalent mineral association *RSDs* (Fig. B.8-9).

The observed preferential associations between Cu-bearing minerals are linked to the formation of rims of secondary bornite, covellite and chalcocite around chalcopyrite grains (Fig. 12.A–D), particularly in the shallow intervals. Hypogene bornite (Fig. 12.E–F) occurs at greater depths in the system (Blannin et al., 2019). It could be expected that the MAMA ratios of chalcopyrite with rim-forming Cu-sulphide minerals should decrease with depth, and that the *RSDs* of these mineral associations be low in the shallow intervals due to the formation of clear rims, and increase with depth. However, no clear trend is seen with depth for the MAMA ratio of any Cu-bearing mineral, and the *RSDs* for chalcopyrite mineral associations with the Cu-bearing sulphides are typically high as a result of the low and variable contents of these minerals. Additionally, the milling process may have made the associations of these minerals less apparent, and the resolution of the MLA cannot clearly define the rims in some cases, as seen by the incomplete rim characterised by MLA in. Fig. 12.A–B.

4.4. Gold deportment

Gold deportment in the Bolcana porphyry system was investigated using a combination of MLA and EPMA. A total of 116 gold grains were identified by MLA, with compositions of < 20 wt% Ag (i.e. electrum), < 10 wt% Ag and high purity Au (Fig. 13). The grains are predominantly electrum, or contain some silver, while a significant number (25) of the identified grains were mixed spectra of gold with either quartz, chalcopyrite or pyrite. For the purpose of simplification, all gold grain compositions were grouped for further interpretation.

Detailed EPMA analyses indicate that Au concentrations in sulphide minerals (pyrite, chalcopyrite, bornite, covellite and chalcocite) are low (< 100 ppm). Note that this is not to say that gold in solid solution in sulphide minerals is negligible, as it may in fact contribute significantly to overall gold deportments (see Appendix A.3 for more details and extended EPMA results). Nevertheless, for the purpose of the subsequent bootstrap resampling calculations, it was assumed that gold hosted by native gold is the dominant mode of occurrence in the Bolcana porphyry system. This assumption was assumed valid as Kesler et al. (2002) confirmed the importance of native gold grains as metal hosts in porphyry copper deposits.

The gold grain size distribution was calculated based on the equivalent circle diameter (ECD) of the grains and is plotted in Fig. 14. Around 67 % of the gold grains are below 4 µm in size, and 90 % below 8 µm. The coarsest gold grain found has an ECD of 22.5 µm. Fine gold is likely to have been characterised reasonably well compared to coarse nuggety gold, which is the hardest to accurately characterise as a result of the enhanced nugget effect. Therefore, the grain size distribution may be skewed to finer grain sizes.

4.5. Gold mineral associations

Due to the low number of gold grains, gold mineral associations were investigated based on individual grains rather than grain mount strips. To prevent over-interpretation of data from samples with few gold grains, the gold mineral associations were only studied for intervals with > 10 gold grains, as well as for a composite of all grains in the 40 m samples (Fig. 15). Gold grains are mainly associated with sulphide minerals, with the remaining associations reflecting the modal mineralogy of the samples.

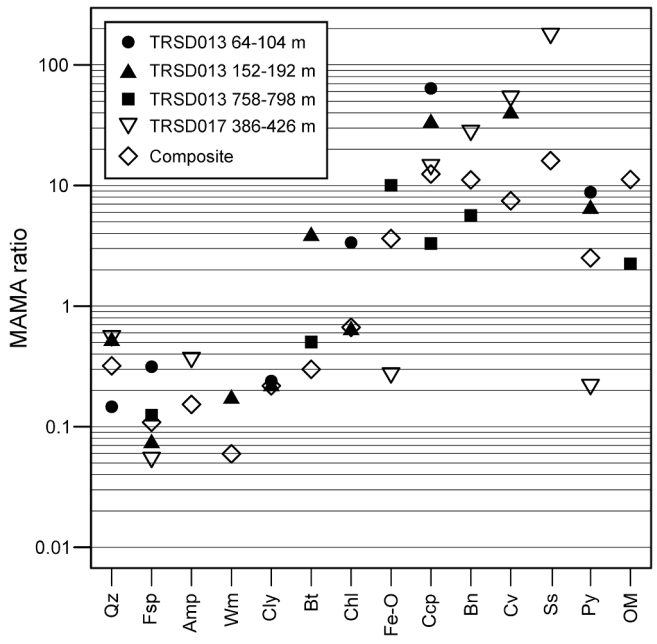

Fig. 16. Median MAMA ratio values of gold for the 40 m interval samples with > 10 gold grains and a composite of all gold grains identified in the 40 m intervals, calculated from the bootstrap resampling results of chalcopyrite mineral associations and modal mineralogy.

The MAMA ratio was calculated to identify preferential associations, with the results plotted in Fig. 16. Gold is preferentially associated with the Cu-sulphide minerals (Fig. 17.A–B,E–H), and pyrite in the near-surface samples (Fig. 17.I–J), with MAMA ratios typically between 5 and 100, similar to the findings of Arif and Baker (2004) and Gregory et al. (2013). There is a high association with Fe-oxide in TRSD013 758–798 m, which is a result of the largest identified gold grain, with an ECD of 22.5 µm, having a large contact area with Fe-oxide (Fig. 17.C–D).

The uncertainties for the mineral associations of gold are very high for most minerals (Figs. 18 and B.10). The lowest *RSD* is typically seen for either free perimeter (11–62 %) or chalcopyrite (14–29 %), as a result of these being the largest and most consistent associations. Therefore, although the uncertainties are quite high, the dominant associations observed are also the most statistically meaningful. The association with pyrite is most notably seen in TRSD013 64–104 m and TRSD013 152–192 m, with *RSD*s of 49 % and 34 % respectively. Overall, the uncertainties for the composite of all gold grains, which includes 90 gold grains, are lower than the individual intervals. The MAMA ratio uncertainties correspond to the mineral association uncertainties (Figs. 19 and B.11).

5. Discussion

In the following, the quality of the MLA-derived quantitative data is assessed. The number of MLA measurements required to provide robust and statistically meaningful data was determined using bootstrap resampling. The implications for process mineralogical and geo-metallurgical studies are discussed accordingly.

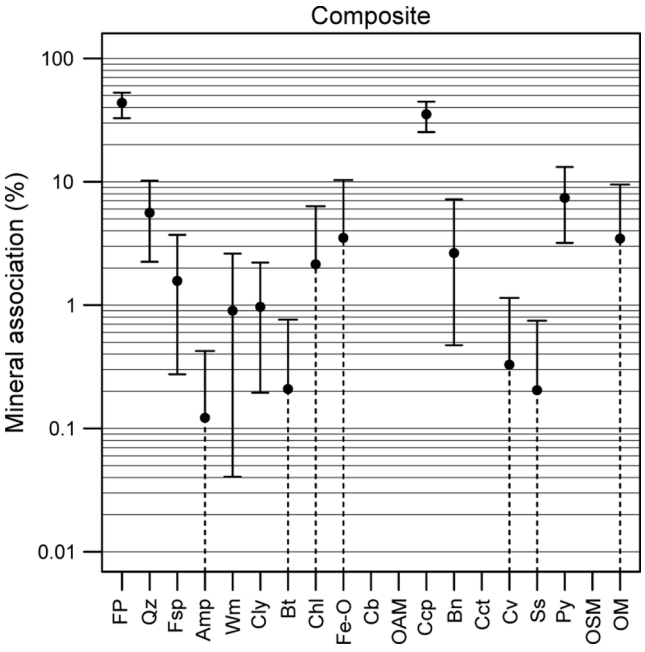

Fig. 18. Median value of bootstrapped gold mineral associations of gold (percentage of gold grain perimeters) for the composite of all 40 m intervals, with 95 % confidence intervals.

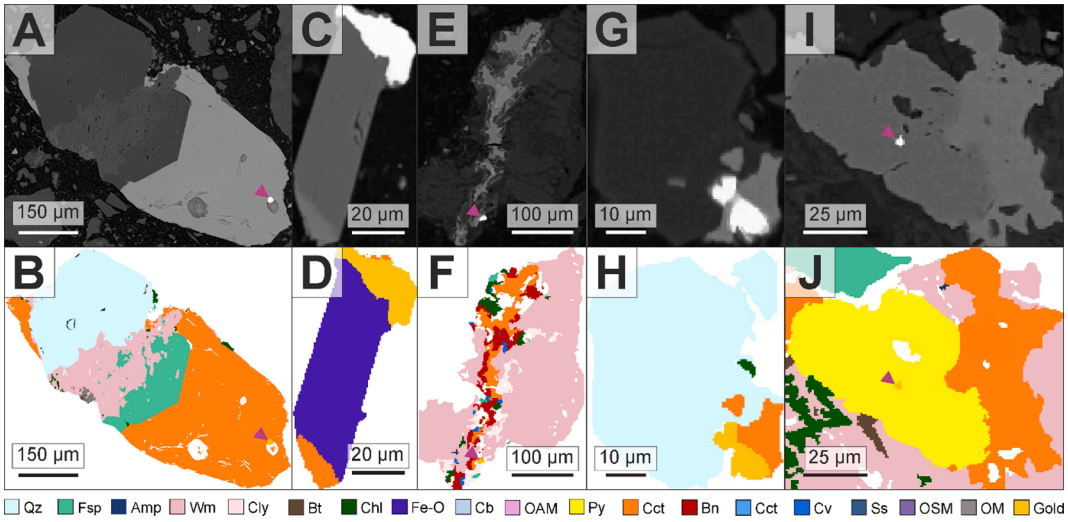

Fig. 17. BSE images (A,C,E,G,I) and false colour images from MLA (B,D,F,H,J) of gold grains in ground samples TRSD017 386–426 m (A,B,G,H), TRSD013 758–798 m (C,D), TRSD013 152–192 m (E,F), and TRSD013 160–164 m (I,J). The gold grain is indicated by a purple arrow-head in A, B, E, F, I and J. The common association of gold grains with chalcopyrite is shown in A–B and E–H, with pyrite in I and J, and with rock-forming and alteration minerals in C–H.

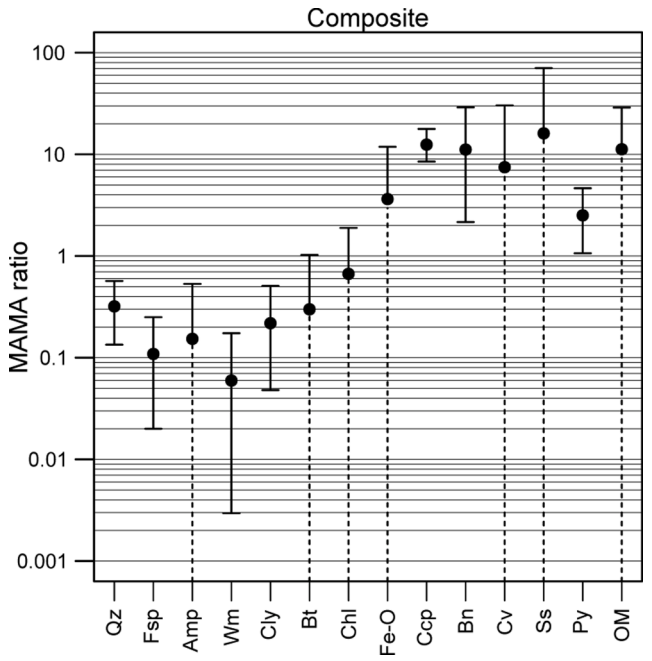

Fig. 19. Median MAMA ratio values of gold for the 40 m interval samples with > 10 gold grains and a composite of all gold grains identified in the 40 m interval, calculated from the bootstrap resampling results of chalcopyrite mineral associations and modal mineralogy, with 95 % confidence intervals.

5.1. Data quality

Limited examples of the application of estimated uncertainties to automated mineralogy studies exist (e.g. Evans and Napier-Munn, 2013; Mariano and Evans, 2015). Accordingly, there are as yet no universally accepted guidelines for acceptable levels of uncertainty in such studies. For the purpose of this study, we therefore decided that *RSD*s of 10 % for modal mineralogy and copper-related measurements would be acceptable, based on industry best-practice (e.g. Dominy et al., 2018) and Gy's formula (Gy, 1982). Of course, in different circumstances, higher or lower uncertainties may be acceptable, depending on the deposit type, the measurement data and the stage of the project. For instance, higher uncertainties are expected for measurements of gold content and textural properties as a results of the nugget effect. We therefore assumed that a *RSD* of 20 % is sufficient for gold. The nugget effect is of course partly a result of the inherent variability of gold grade in the deposit, but sample size, preparation and analysis can contribute significantly to the total nugget effect (e.g. Clark, 2010; Dominy et al., 2003; 2001; Dominy and Edgar, 2012).

The use of Gy's formula (Gy, 1982) to guide sampling of particulate material is well-established, particularly for trace elements, such as gold, where the nugget effect may be very pronounced and detailed planning is required to minimise errors during sampling and subsequent sub-sampling and sample preparation steps. However, such error estimates are often not considered when finally taking analytical samples, such as for automated mineralogy purposes. Based on the material properties of the studied samples, Gy's formula suggests that around 1000 g of sample would be required for a *RSD* of 20 % for Au content, in stark contrast to the 0.2 g required for an *RSD* of 10 % for chalcopyrite grade. One grain mount contains around 1 g, or less,of sample material. The *RSD* of taking 1 g of the material is around 4.5 % for chalcopyrite, but around 600 % for gold. However, when only one surface of the grain mount is measured, the equivalent mass measured by MLA will be only a small fraction of this. This raises the question of the overall representativity of such samples.

To assess the quality and reliability of the MLA measurements, calculated Cu and Au grades were compared with the chemical assays provided by Deva Gold S.A. for the same samples (Fig. 20). Despite different mineralisation styles and variable mineralogy, the general agreement between the chemical and calculated assays for Cu is very good (Fig. 20.A). The Cu contents calculated for the 40 m intervals show no systematic over- or under-estimation of Cu grade, and all plot on, or close to, the 1:1 line within error. The *RSD*s of the calculated Cu contents in the 40 m samples vary between around 3 % and 8 % and are thus deemed acceptable. All 4 m samples from TRSD013 152–192 m also lie on the 1:1 line within error, although the uncertainties are larger than for the 40 m interval samples, with *RSD*s between around 3 % and 11 %. The higher variability recorded for the 4 m samples, relative to the 40 m interval samples, is mostly related to fewer strips being available for re-

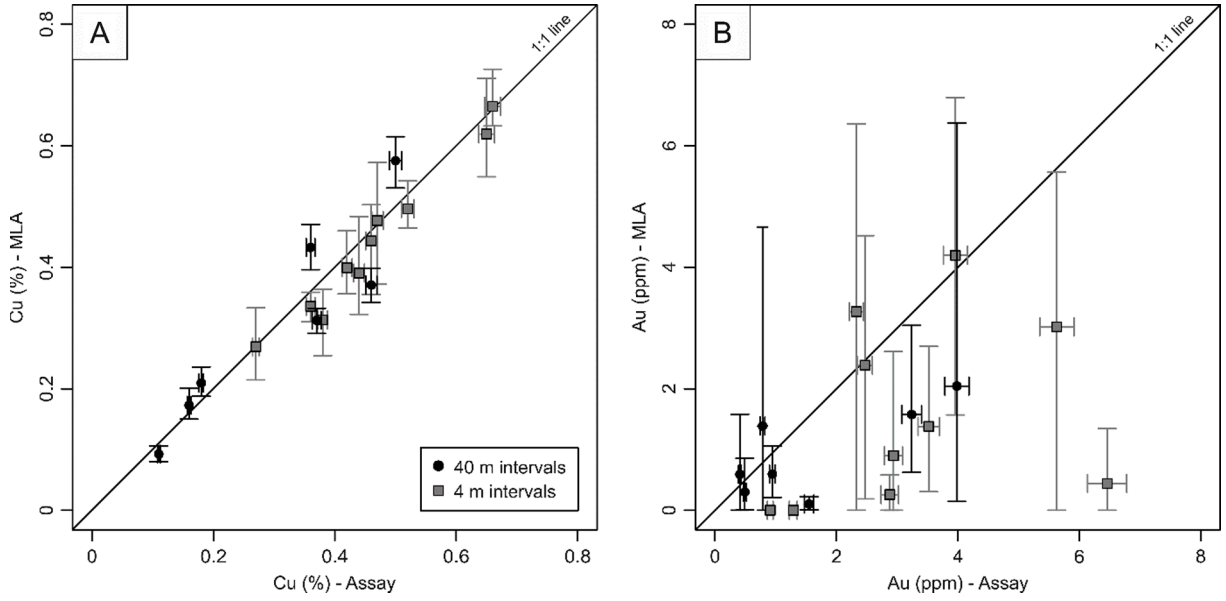

Fig. 20. Plots of calculated Cu (left) and Au (right) contents from MLA versus the Cu and Au contents measured by chemical assays. Both the 40 m crushed material samples and the 4 m crushed material samples from TRSD013 152–192 m are plotted, with composite values for each. The errors of the MLA data were estimated by bootstrap resampling, to give 95 % confidence intervals. The errors on the chemical assay values were estimated based on blanks, standards and duplicate samples, to give around ± 2 % for Cu and ± 5 % for Au.

Table 4
The number of grain mount surfaces required to characterise different properties with an *RSD* of 10 % (modal mineralogy, Cu content and chalcopyrite mineral associations) or 20 % (Au content) for each 40 m interval sample, as estimated by bootstrap resampling.

	TRSD013				TRSD017		
	64–104 m	152–192 m	356–396 m	758–798 m	240–280 m	346–386 m	386–426 m
Cu content	1	2	6	2	3	3	1
Au content	21	20	80	44	75	124	90
Modal mineralogy[*1]	7	8	5	6	6	38[*2]	5
Ccp mineral associations[*3]	8	7	24	37[*4]	15	29[*5]	26

[*1] Including minerals with an abundance of > 5 wt% and Cu-bearing minerals which contribute > 10 % of Cu deportment – Qz, Fsp and Ccp for all samples, Wm for all samples except TRSD013 152–192 m, Cly for TRSD013 64–104 m and TRSD013 152–192 m, Chl for all samples except TRSD013 64–104 m, Bt for TRSD013 758–798 m and TRSD017 346–386 m, Fe-O for TRSD013 758–798 m, TRSD017 346–386 m and TRSD017 386–426 m, Py for TRSD017 240–280 m, Bn for TRSD013 64–104 m, TRSD013 758–798 m and TRSD017 346–486 m, Cv for TRSD013 64–104 m, and Cct for TRSD017 346–386 m.
[*2] Bn requires 10 surfaces and Cct requires 38, but the remaining dominant minerals require only 5 surfaces.
[*3] Including minerals with an association of over 5 % with chalcopyrite – Qz, Fsp, Wm, Py and FP for all samples, Cly for TRSD013 64–104 m and TRSD013 152–192 m, Chl for all samples except TRSD013 64–104 m and TRSD017 386–426 m, Fe–O TRSD017 346–386 m and TRSD017 386–426 m, Bn for TRSD013 64–104 m, TRSD013 758–798 m and TRSD017 346–386 m and Cct for TRSD017 346–386 m.
[*4] Excluding Py which required > 50 surfaces.
[*5] Excluding Cct which required > 50 surfaces.

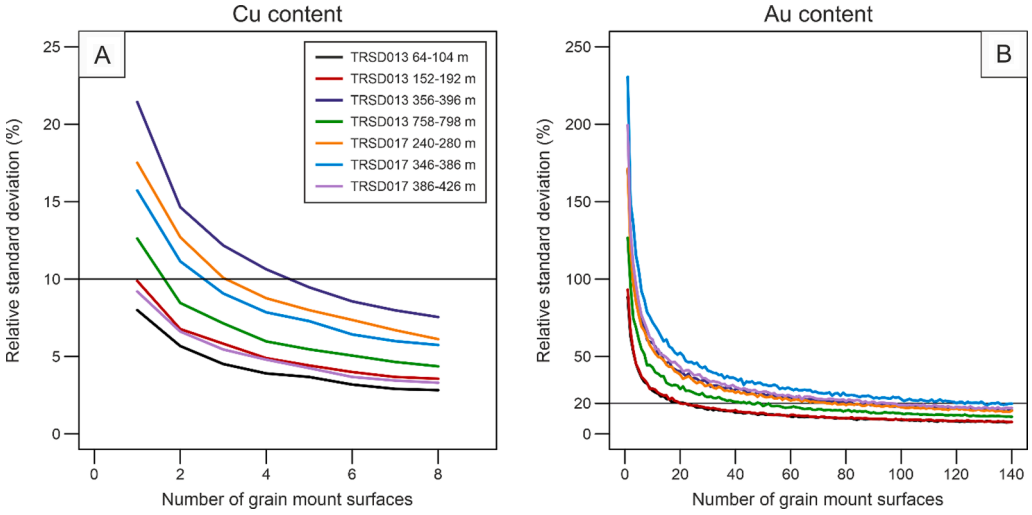

Fig. 21. Bootstrap resampling of Cu content (A) and Au content (B) calculated from MLA data, for all 40 m interval samples. The resampling was carried out by increasing ***N*** in increments of 5, to represent a single grain mount surface composed of 5 strips, until the *RSD* decreased to 10 % for Cu content and 20 % for Au content, for all intervals.

sampling during the bootstrapping procedure.

For Au, on the other hand, estimated uncertainties of the calculated assays for individual samples are very high (Fig. 20.B). The *RSD*s for the 40 m intervals range from 36 to 88 %, and between 31 and 84 % for the 4 m samples. No clear systematic relationship is apparent between calculated and chemical assays. However, it can be noted that median calculated concentrations are often well below measured concentrations. Only in rare cases do calculated Au contents exceed the chemical assay results by a minor amount. The discrepancy in Au measurements is likely a result of the low overall concentrations of Au and the low and variable numbers of grains present in each section, leading to a pronounced nugget effect. However, it is also possible that a considerable amount of gold may be hosted in sulphide minerals, as previously discussed and shown in Appendix A.3.

Table 5
Number of gold grains needed to reach a *RSD* of 20 % for mineral associations of all gold in the 40 m interval crushed material samples, for minerals with associations > 5 % when free perimeter is excluded. ***N*** was increased in increments of 5 up to 700 for the bootstrap resampling, to reach the required *RSD*. The number of grain mount surfaces required to reach the required *RSD* was calculated assuming that two gold grains are present in each grain mount surface.

	FP	Qz	Ccp	Bn	Py
No. Au grains	45	240	45	690	225
No. grain mount surfaces	23	120	23	345	113

5.2. Implications for analytical work

Uncertainties on all MLA-derived textural data estimated by bootstrap resampling provide a valuable insight into the reliability of the data (Evans and Napier-Munn, 2013; Mariano and Evans, 2015). In this study, six measured grain mount surfaces were sufficient to give reliable results for Cu content with MLA, but not for Au content (Fig. 20). For the majority of the textural measurements of the 40 m samples, the *RSD*s were acceptable for major minerals, such as the dominant minerals in the modal mineralogy, the Cu deportment and the major chalcopyrite mineral associations. The high uncertainties encountered for the textural properties and contents of minor minerals could have been expected. However, this information is typically not significant for geometallurgical modelling and ore processing, except in the case of gold, where these measurements are of course important and the higher uncertainties are problematic.

The question remains, how many sample surfaces would need to be measured to yield reliable results for quantities, such as Au content that

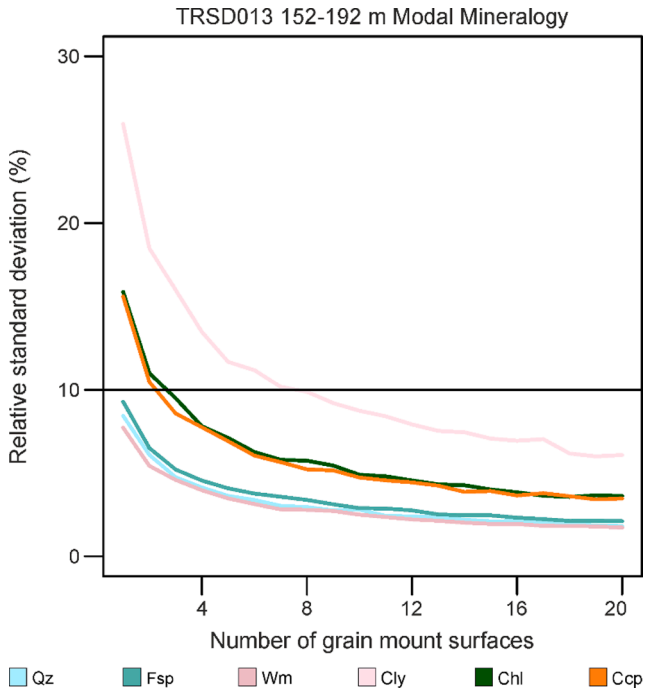

Fig. 22. Bootstrap resampling of modal mineralogy of the TRSD013 152–192 m sample for minerals with an abundance of > 5 wt% and Cu-bearing minerals which contribute > 5 % of Cu deportment. ***N*** was increased in increments of 5, to represent a single grain mount surface composed of 5 strips, until the required *RSD* of 10 % was reached for all minerals.

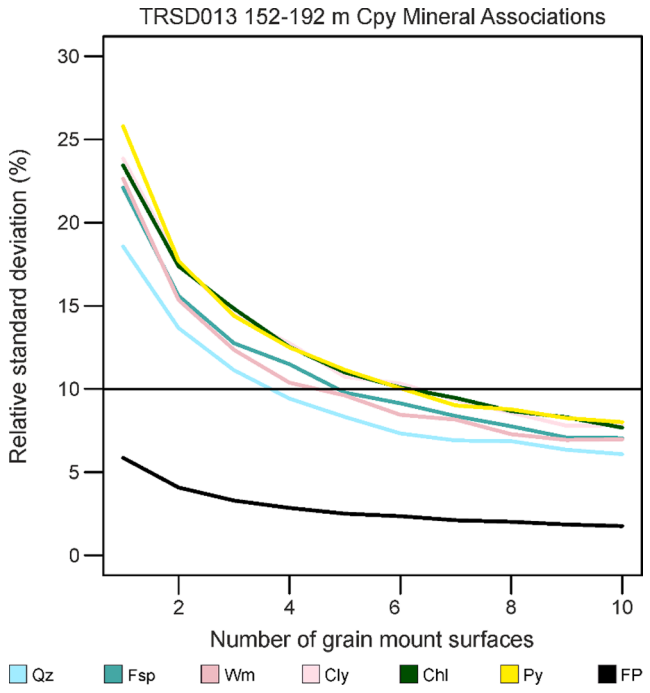

Fig. 23. Bootstrap resampling of mineral associations of chalcopyrite in the TRSD013 152–192 m sample for minerals with an association of > 5 % when ignoring free perimeter. ***N*** was increased in increments of 5, to represent a single grain mount surface composed of 5 strips, until the required *RSD* of 10 % was reached for all minerals, or to a limit of 50 surfaces.

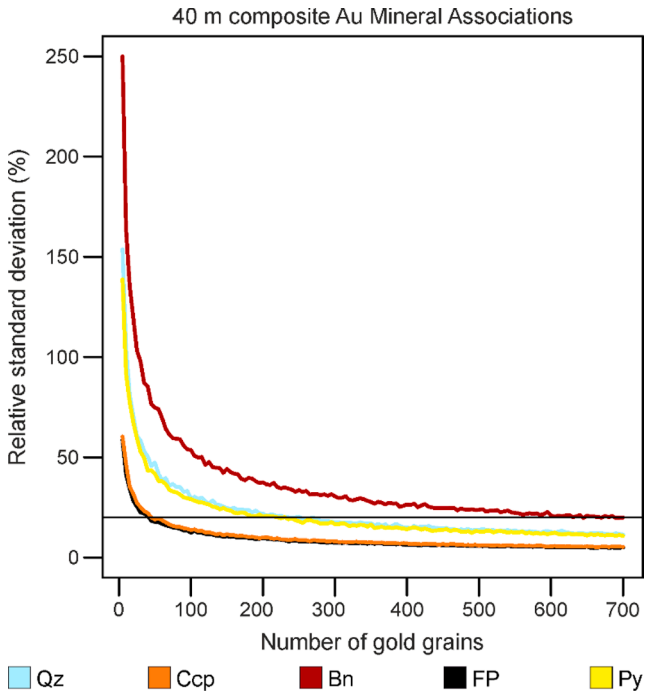

Fig. 24. Bootstrap resampling of the mineral associations of all gold grains in the 40 m samples, for minerals with > 5% association. The number of gold grains was increased in increments of 5 up to 700 for the bootstrap resampling, to reach the required *RSD* of 20 %.

were not reliably constrained by the current dataset. To answer this question, further bootstrap resampling was performed to find the number of grain mount surfaces required to provide statistically robust results for the important geometallurgical properties of Cu content, Au content, modal mineralogy and chalcopyrite and gold mineral associations with the results summarised in Table 4.

Similar to the findings of Evans and Napier-Munn (2013), who reported the area of particles to be measured, the copper content calculated by MLA mainly required 1–3 grain mount surfaces to be analysed for an *RSD* of 10 % (Fig. 21.A). However, for the 40 m sample with the lowest Cu content (< 0.2 % Cu), 6 surfaces are required (Table 5, Fig. 21.A). The minimum number of grain mount surfaces required to characterise Au content with an *RSD* of 20 % is 20, while the maximum is 124 surfaces (Table 5, Fig. 21.B). There is no clear relation between the expected gold content and the number of surfaces to be measured.

The modal mineralogy of the 40 m interval samples was bootstrap resampled to achieve acceptable results for minerals with an abundance of > 5 wt% and Cu-bearing minerals which contribute > 10 % of Cu deportment (Figs. 22 and C.1, Table C1). Overall, analyses of up to around 3 surfaces are required to accurately characterise the dominant mineral groups. When also considering the Cu-bearing minerals, the number of surfaces required increases up to 6 for chalcopyrite, 15 for bornite, and 38 for the other Cu-sulphides. When accounting for minor Cu minerals, the number of surfaces required may almost be the same as for gold due to their low abundance. In such cases, it may be more appropriate to accept a higher *RSD*.

Mineral associations of the valuable minerals are important to consider in geometallurgical studies. Measurements of between around 7 and 37 grain mounts surfaces are required to achieve *RSD*s of < 10 % for the dominant mineral associations, i.e. minerals with an association of over 5 % with chalcopyrite (Figs. 23 and C2, Tables 5 and C2). Free perimeter requires only a single surface for all samples. The number of surfaces required tends to correlate with the chalcopyrite content, with some exceptions, e.g. TRSD13 758–798 m, which may be a function of texture and grain size. Due to their low contents, pyrite in TRSD013

758–798 m and chalcocite in TRSD017 346–386 m would require > 50 surfaces to be analysed for *RSD*s of < 10 %. Again, it will be necessary to determine which mineral associations may be most beneficial or problematic, and ensure that these associations can be characterised to an acceptable confidence limit. MAMA ratio uncertainties are closely related and therefore can be assumed to follow the same trends as the mineral associations.

The dominant mineral associations, i.e. those with associations > 5 %, of all gold grains in the 40 m samples were bootstrap resampled (Table 5, Fig. 24). The gold grains in the 4 m samples from TRSD013 152–192 m were excluded to prevent over-representation of this interval. The uncertainties for individual intervals were assumed too high to provide meaningful insights. A very large number of gold grains are necessary to provide robust statistics of the mineral associations for most minerals, even for the main mineral associations which are assessed here. Free perimeter and chalcopyrite require around 45 grains for an *RSD* of 20 %, compared to 225 for pyrite, 240 for quartz and up to almost 700 for bornite. Considering that 90 gold grains were identified in 42 grain mount surfaces, equating to around two gold grains per surface, around 345 grain mount surfaces would be needed to identify a sufficient number of gold grains to reach the required *RSD*. When considering the individual 40 m samples, the number of surfaces to be measured would increase even further.

The increase in uncertainties on textural measurements resulting from low mineral grades, which was clearly observed in this study, can be expected from theoretical principals e.g. Gy (1982). Mariano and Evans (2015) analysed samples from rougher flotation of an iron oxide Cu-Au ore, sieved into 5 size fractions. Although it was illustrated that *RSD*s on measurements reduce with decreasing particle size, the –75 +38 μm fraction of the low grade sample has *RSD*s from around 20 to over 100 % for the distribution of pyrite liberation classes. Conversely, for the same measurements of the same size fraction of a high grade sample, not even a whole grain mount surface was required to reach an acceptable *RSD* of 10 %. When combining the effects of low grade and grain size, the measurement uncertainties are sure to increase. Assuming that coarser size fractions are the major source of uncertainties, measuring multiple size fractions may reduce measurement uncertainties for coarser size ranges at least, but the effect of grade cannot be ignored. Overall, the influence of size fractions has not been clearly shown in this study.

5.3. Consequences for geometallurgical programmes

Geometallurgical programs requiring the textural data provided by automated mineralogy typically analyse large numbers of samples. Although it is common practise to analyse duplicate samples, which would allow estimations of measurement errors, duplicates may be sacrificed in order to investigate as many different ore types as possible. Even if this was not the case, the present analysis showed that duplicate measurements are generally not sufficient to characterise many important parameters with an acceptable degree of accuracy. This is particularly true for gold contents and mineral associations. In an industrial setting, it would simply not be feasible to analyse > 124 grain mount surfaces for one single sample, as has been shown necessary to accurately characterise gold content in some cases. This would require a large amount of sample material, and time and money for sample preparation, analysis, and data processing. As a consequence, it may be necessary to concede that minerals present in minor amounts may never be measured quantitatively by automated mineralogical techniques, with the results being semi-quantitative at best, and perhaps only qualitative.

Given these results, there must be a cost-benefit analysis to decide how many measurements should be performed to reduce uncertainties to an acceptable value. Decisions must also be made on what textural properties are most important for ore processing, and what uncertainties are acceptable. For example, high *RSD*s should only be considered critical if they are observed for combinations of ore minerals with abundant gangue minerals. Any combination of rare ore mineral with rare gangue mineral will yield elevated *RSD*s, but this is typically irrelevant for processing decisions and can therefore be ignored.

Ore textures also influence the complexity of accurate characterisation and therefore certain textures could be expected to contribute to higher uncertainties. For instance, samples with finely inter-grown minerals are much more challenging to characterise than coarse mineral grains. Strategies such as including mixed spectra in the mineral list are commonly implemented to tackle the high abundance of mixed spectra resulting from finely intergrown textures (e.g. Kern et al., 2018). However, this approach is not always straightforward and requires careful processing of the data to ensure that uncertainties remain low. The measurement mode plays an important role in the quality of the data obtained for complex textures. This becomes particularly important when ore minerals of interest are very fine-grained, such as the gold grains identified in this study. To improve the data quality it may be necessary to use more accurate and time-consuming measurement modes, or combinations of measurement modes, at high resolution (e.g. GXMAP, Fandrich et al. (2007)) in order to identify finer grains and reduce the generation of mixed spectra. However, this study encountered large uncertainties in the Au measurements, even when combining two of the most accurate modes: GXMAP with SPL. Additionally, measurements of some textural characteristics, such as mineral liberation, require time-intensive measurement modes where entire particles are scanned rather than simpler and faster line scans. As previously stated, decisions must be made ahead of time about which textural properties are the focus of a study, followed by a weigh-up of the costs and benefits of different measurement modes.

While this study only measured one size fraction, −600 μm, it would perhaps be preferable to sieve each sample into several size fractions. This strategy is often applied in geometallurgical programmes to reduce uncertainties by measuring a higher number of particles for each size fraction. This is particularly relevant for larger size fractions, where uncertainties are typically significant (Mariano and Evans, 2015). This should also result in a reduction of uncertainties related to the cut-effect, i.e. the fact that the true particle sizes in a grain mount are not known and the observed sizes give only a lower bound. However, the separate analysis of several size fractions also directly implies the preparation of several grain mounts per sample. Unless some optimisation is done with respect to the number of grain mounts to be measured for each size fraction, this may in fact lead to greater preparation and measurement costs of a geometallurgical programme than if samples are prepared without prior sieving. Coarser size fractions may still require multiple grain mounts to be prepared for reasonable measurement uncertainties, increasing the number of analyses further. Unfortunately, the authors are not aware of any rigorous comparative study assessing the relative benefits of both approaches to sample preparation. Therefore, it is difficult to say which provides the greater benefits for the improvement of measurement statistics.

The contents, associations and uncertainties of the major minerals, as well as those of chalcopyrite, the main Cu-bearing mineral, are generally well-constrained. However, some samples have consistently higher uncertainties than others (e.g. TRSD017 346–386 m as seen in Table 5). In other cases, certain textural properties are less well constrained (e.g. chalcopyrite mineral associations in TRSD013 758–798 m as seen in Table 5). As can be seen in Table 1, the studied 40 m intervals comprise different lithologies and styles of alteration and mineralisation. Considering this, it is perhaps not surprising that some mineral contents and textural properties exhibit variable uncertainties, albeit far less so than the Au deportment. It is imperative for reliable results of process mineralogical and geometallurgical studies, that sampling strategies should be designed to reduce uncertainties at the earliest stage. For instance, if large intervals are selected for analyses, where high variability can already be expected due to combinations of different lithologies, alteration and mineralisation styles, of course the uncertainties in the following analyses will be large. Instead, sampling schemes should

be designed, with the theory of sampling in mind, to focus on domains of lithology, mineralisation, alteration etc., which are relatively homogeneous within the interval.

Bootstrap resampling clearly provides an effective tool for the determination of uncertainties (Evans and Napier-Munn, 2013; Mariano and Evans, 2015). The routine application of bootstrapping error assessments should become the norm, with estimated errors being clearly stated to ensure that any technical decisions take uncertainty of the results into account. However, bootstrap resampling alone cannot replace duplicate analyses. Therefore, the sampling strategy, including running of duplicates at regular intervals, should be carefully planned and implemented at all stages.

6. Conclusions

Quantitative automated mineralogy methods have been, and will continue to be, invaluable for many reasons. While great advances have been made in the field since their advent, the statistical uncertainties accompanying the results, which were given much consideration during the early development of these methods (e.g. Butcher et al., 2000; Gottlieb et al., 2000), seem to have been somewhat sacrificed for the speed and cost of the measurements. An in-depth study into uncertainties associated with automated mineralogy-based metal deportment and mineral association studies has been conducted to illustrate the need for the inclusion of error estimates, particularly for geometallurgical studies where technical decisions may be made based on the data. Such uncertainty assessments can be readily conducted on all relevant textural parameters using the bootstrap resampling method. Different minerals could also be studied, although caution must be taken with minerals present in low concentrations, as clearly illustrated by the high uncertainties for gold measurements in comparison to chalcopyrite. Additionally, the method is not limited to the specific case study of a porphyry Au-Cu deposit, but should be directly transferrable to any deposit type, including both primary and secondary deposits such as mine and metallurgical wastes.

Despite different mineralisation styles and variable mineralogy, estimated statistical uncertainties on Cu content and mineral associations are low for the selected case study, a low-grade Cu-Au porphyry system with concentrations of Cu well below 0.5 wt%. The same cannot be said for Au content and mineral associations, which have very large uncertainties. This is, of course, attributed to the very low concentration of gold, the low number of gold-bearing mineral grains and the nugget effect. Critically, our results show that the attainment of acceptable uncertainties for metal grades does not necessarily imply that the same is the case for other important parameters such as deportment or mineral association. To constrain these characteristics, more data is typically needed.

Although it was determined that up to 5 grain mount surfaces would be sufficient to provide robust measurement statistics in most cases, this is still a large number of measurements for a single sample for any geometallurgical programme. In short, the selection of samples which are representative of a whole ore deposit, while minimising time, cost and importantly uncertainties on the textural parameters of interest is still challenging. It should become the industry norm that such assessments of uncertainties come hand-in-hand with automated mineralogy-based studies, to ensure that meaningful interpretation is possible. Great care should be taken first when planning sampling schemes and automated mineralogy studies, and when subsequently reporting analytical results, especially for precious metals and trace minerals which will generally show higher uncertainties.

CRediT authorship contribution statement

Rosie Blannin: Conceptualization, Methodology, Software, Validation, Formal analysis, Investigation, Data curation, Writing - original draft, Writing - review & editing, Visualization. **Max Frenzel:** Conceptualization, Validation, Writing - review & editing. **Laura Tusa:** Investigation, Writing - review & editing. **Sandra Birtel:** Writing - review & editing, Supervision. **Paul Ivăscanu:** Resources, Writing - review & editing, Supervision. **Tim Baker:** Resources, Writing - review & editing. **Jens Gutzmer:** Conceptualization, Writing - review & editing, Supervision.

Declaration of Competing Interest

The authors declare that they have no known competing financial interests or personal relationships that could have appeared to influence the work reported in this paper.

Acknowledgements

We would like to acknowledge the anonymous reviewer for their constructive comments and valuable insight. Sabine Gilbricht (TU Bergakademie Freiberg), Kristine Trinks (HZDR) and Kai Bachmann (HZDR) are thanked for their support during SEM-MLA data acquisition. Joachim Krause (HZDR) is acknowledged for EPMA data acquisition and processing. The sample preparation staff at the Helmholtz Institute Freiberg for Resource Technology are thanked for the great help in preparing the samples. The first author would like to thank the European Union's Erasmus Mundus Program for a scholarship of the Emerald MSc program. In addition, the completion of the paper was supported by the SULTAN project. This project has received funding from the European Union's EU Framework Programme for Research and Innovation Horizon 2020 under Grant Agreement No 812580.

Appendix A

Electron microprobe analysis method

EPMA analyses were carried out at HIF, using a JEOL JXA-8530F EPMA equipped with five wavelength dispersive spectrometers and a field emission electron gun. Twenty-one elements were analysed on 585 points (including standard blocks for major elements every ~ 160 points), each with a measurement time of eight and a half minutes, using an acceleration voltage of 20 Kv and a probe current of 35 nA.

Mineral grains suitable for measurement were identified using the MLA GXMAP results of samples TRSD013 64–104 m, TRSD017 386–426 m and TRSD013 758–798 m and TRSD013 184–188 m. Grains of gold, pyrite, chalcopyrite, bornite, covellite and/or chalcocite were bookmarked. The measurement points were efficiently located with the point logger, the coordinates recorded and transferred to the EPMA (cf. Osbahr et al. 2015). The grain mounts were coated twice with graphite to reduce the likelihood of surface charging. The measurement settings are found in Table A1.

During and after data acquisition, online and offline corrections were performed: (1) an offline overlap correction method, based on weight proportions of elements present (cf. Osbahr et al. 2015); (2) background corrections to remove the contribution from the background to the measured peak intensity (Lavrent'ev et al., 2015; Osbahr et al., 2015; Reed, 2005); (3) a drift correction, carried out using the standard measurements. The corrected measurements were filtered for values below the quantification limit, and analytical errors exceeding 10 %. Measurements with totals of 100 ± 1.5 % were retained. The stoichiometry of the minerals measured was calculated for S, Fe and Cu and filtered for errors of > 10 % for pyrite and chalcopyrite and > 15 % for bornite and chalcocite and covellite.

Copper deportment

The mineral chemistry of chalcopyrite, bornite, covellite and chalcocite were measured with EPMA in four grain mounts (TRSD013

64–104 m, 184–188 m, 758–798 m and TRSD017 386–426 m). The stoichiometric compositions of the measured minerals were calculated, based on the Fe, S and Cu contents (Table A2). It can be seen that there are far fewer valid measurements for bornite, chalcocite and covellite compared to chalcopyrite. This is partly because they occur at lower abundances, but also because the surfaces of the minerals were often altered and good measurements could not be taken. Despite this, no systematic bias in measurements for a specific mineral composition was detected. Therefore, the EPMA results validate the use of the standard stoichiometric mineral formulae to calculate copper deportment.

The average areas of the copper-bearing minerals are given in Table A3, for each 40 m and 4 m interval sample. The area of chalcopyrite is one or two orders of magnitude greater than bornite, chalcocite, covellite and sulphosalts. This clearly illustrates the dominance of chalcopyrite in the copper deportment of all samples.

Gold deportment

EPMA was used to analyse the composition of two gold grains in sample TRSD013 184–188 m (Table A3). These have molar Au:Ag ratios of 12.7 to 94.1, corresponding to the Ag contents detected by MLA (Fig. 13).

In this study, gold is assumed to be mainly hosted by gold grains. However, significant amounts of gold could be hosted by sulphide minerals in solid solution, as is common in porphyry deposits (e.g. Arif and Baker, 2004; Gregory et al., 2013; Kesler et al., 2002; Simon et al., 2000)). However, detailed EPMA analyses indicate that Au is absent in concentrations close to, or above, the detection limit of around 100 ppm in all measured sulphides (pyrite, chalcopyrite, bornite, covellite and chalcocite). In contrast, Cioacă et al. (2014) estimated that samples from the Bolcana system contained, on average, 46 ppm Au in pyrite, 108 ppm Au in chalcopyrite and 116 ppm Au in bornite, from EPMA studied. Limited information can be inferred from this as a result of the samples being from different locations in the Bolcana system.

To provide an estimate of how much gold may be hosted by sulphides in the studied samples, it was assumed that pyrite, chalcopyrite and bornite could host up to 50 ppm Au in solid solution, i.e. half the detection limit of 100 ppm (Table A4). The estimated total content of gold in solid solution varies between 0.5 and 2.9 ppm. However, when compared to the 'missing' gold, i.e. the difference between the gold calculated assay from MLA and the chemical assay, the estimate of solid solution gold generally exceeds the 'missing' gold and therefore it is likely an over-estimate. As a result, for the purpose of deportment calculations, it was thus assumed that gold contents in these sulphide minerals are negligible. Following this assumption, gold deportment in all studied samples is limited to the presence of native gold grains. However it is still likely that gold occurs in solid solution in some sulphide minerals, in variable amounts throughout the different intervals due to varying styles of mineralisation, over-printing, alteration and lithologies.

See Table A1, Table A2, Table A3, Table A4, Table A5

Table A1
Analytical conditions for EPMA analysis (Spectr = spectrometer; Peak pos. = peak position; Lower backgr. = lower background; Upper backgr. = upper background; Meas. time peak = measurement time peak; Meas. time backgr. = measurement time background; Quant. limit = quantification limit). Standards supplied by ASTIMEX Standards Ltd.

Element/ Line	Spectr./ Crystal	Peak pos. (mm)	Lower backgr. (mm)	Upper backgr. (mm)	Meas. time peak (s)	Meas. time backgr. (s)	Quant. limit (ppm)	Standards
Si Kα1	1 TAP	77.311	/	5.565	20	10	99	Plagioclase_AST
Al Kα1	2 TAP	90.584	6.858	9.337	20	5	129	Plagioclase_AST
As Lα1	3 TAP	105.132	6.127	2.286	60	15	200	Arsenopyrite_AST
Se Lα1	1 TAP	97.678	5.588	3.06	60	15	222	BismuthSelenite_AST
Sn Lα1	2 PETJ	114.97	1.976	6.644	80	20	262	Tin_AST
Ag Lα1	2 PETJ	132.697	5.219	1.874	120	30	300	Silver_AST
S Kα1	2 PETJ	171.637	/	4.942	20	10	230	Sphalerite_AST
Hg Mα1	2 PETJ	180.36	3.949	9.307	60	15	751	Cinnabar_AST
In Lα1	3 PETL	121.114	16.693	8.014	160	15	192	IndiumPhospide_AST
Cd Lα1	3 PETL	126.98	/	2.463	60	30	115	Cadmium_AST
Au Mα1	3 PETL	187.002	10.418	9.281	180	45	304	Gold_AST
Zn Kα1	4 LIFH	99.99	4.963	5.016	40	10.5	300	Sphalerite_AST
Cu Kα1	4 LIFH	107.345	1.96	2.131	30	7.5	290	Copper_AST
Fe Kα1	4 LIFH	134.885	5.1	3	30	7.5	217	Pentlandite_AST
Co Kα1	4 LIFH	124.647	3.106	2.745	60	15	187	Cobalt_AST
Te Kα1	4 PETH	105.15	10.989	7.96	80	20	107	Tellurium_AST
Sb Lβ1	4 PETH	103.143	8.361	/	40	20	343	Stibnite_AST
Ni Kα1	5 LIFH	115.396	5.397	4.581	40	10	238	Pentlandite_AST
Mn Kα1	5 LIFH	146.333	2.479	5.177	40	10	194	Rhodonite_AST
Bi Mβ1	5 PETH	157.205	5.125	18.723	60	15	325	BismuthSelenite_AST
Pb Kα1	5 PETH	169.255	/	7.835	40	20	266	Galena_AST

Table A2
Stoichiometric compositions of Cu-bearing sulphide minerals, as calculated from EPMA results. *n* = number of valid measurements (total of 98.5–100.5 wt%, error of < 10 % in stoichiometry for chalcopyrite, and < 15 % for bornite, chalcocite and covellite), Med. = median value and STD = standard deviation. Note that the low number of valid measurements for bornite, chalcocite and particularly covellite mean that the standard deviation is not as statistically meaningful as for chalcopyrite.

Mineral	n	S		Fe		Cu	
		Med.	STD	Med.	STD	Med.	STD
Ccp	92	2.2	0.02	1.2	0.01	1.2	0.01
Bn	7	1.6	0.04	0.4	0.03	2.2	0.05
Cct	5	1.4	0.09	0.1	0.04	2.6	0.07
Cv	2	1.5	0.02	0.1	0.05	1.3	0.03

Table A3
The average area (mm^2) of Cu-bearing minerals identified by MLA in the six measured grain mount surfaces of each 40 m interval sample, and the one measured surface for the 4 m interval grain mounts from TRSD013 152–192 m. No value indicates that the mineral was not identified, or the average area of the given mineral was < 0.001 mm^2. The average area of gold is given in μm^2 rather than mm^2, with 1 μm^2 equalling 1e-6 mm^2.

	TRSD0S13				TRSD0S17			TRSD013 152–192 m interval 4 m samples									
	64–104 m	152–192 m	356–396 m	758–798 m	240–280 m	346–386 m	386–426 m	152–156 m	156–160 m	160–164 m	164–168 m	168–172 m	172–176 m	176–180 m	180–184 m	184–188 m	188–192 m
Ccp	0.31	0.41	0.14	0.51	0.18	0.13	0.78	0.32	0.39	0.70	0.53	0.96	0.89	0.38	0.34	0.57	0.29
Bn	0.017	0.012	0.002	0.067	0.003	0.017	0.02	0.001	0.001	0.008	0.002	0.008	0.002	0.007	0.02	0.05	0.01
Cct				0.003	0.003	0.012	0.003										
Cv	0.018	0.015		0.008	0.002	0.007	0.005		0.001	0.001	0.005	0.005		0.01	0.05	0.05	0.03
Ss	0.003	0.005			0.003		0.002	0.06	0.007				0.002		0.004	0.004	0.002
Au	11.20	39.13	5.99	147.27	6.18	16.41	96.42			1.24	7.42	0.78	8.72	7.49	0.91	8.72	1.95

Table A4
EPMA results of valid measurements of gold grains (total of 100 ± 1.5 wt%). Elements with 0 content were removed from the table.

Measurement code	Measured elemental composition (wt%)							Molar Ratio Au:Ag
	Si	Ag	Cd	Au	Cu	Fe	Total	
184_188 Gold 2	0.12	0.63		99.1	0.90	0.57	101.3	94.1
184_188 Gold 3	0.13	4.50	0.04	95.8		0.34	100.8	12.7

Table A5
Potential concentrations of Au hosted by pyrite, chalcopyrite and bornite in each 40 m interval, assuming concentrations of 50 ppm Au in each mineral. The value of 'missing' gold (i.e. the difference between the MLA calculated assay and the chemical assay) is given for comparison, except for TRSD013 356–396 m and TRSD017 386–342 m, where the Au content calculated from the MLA results exceeds the chemical assay.

	TRSD013				TRSD017		
	64–104 m	152–192 m	356–396 m	758–798 m	240–280 m	346–386 m	386–426 m
Pyrite	2.1	1.5	0.9	0.5	2.7	0.3	0.9
Chalcopyrite	0.4	0.5	0.8	0.5	0.2	0.2	0.8
Bornite	0.02	0.02	0.02	0.1	0.01	0.03	0.02
Total	2.5	2.0	1.7	1.0	2.9	0.5	1.7
'Missing' Au	0.4	1.7	–	1.9	0.2	1.4	–

Appendix B

See Fig. B1, Fig. B2, Fig. B3, Fig. B4, Fig. B5, Fig. B6, Fig. B7, Fig. B8, Fig. B9, Fig. B10, Fig. B11

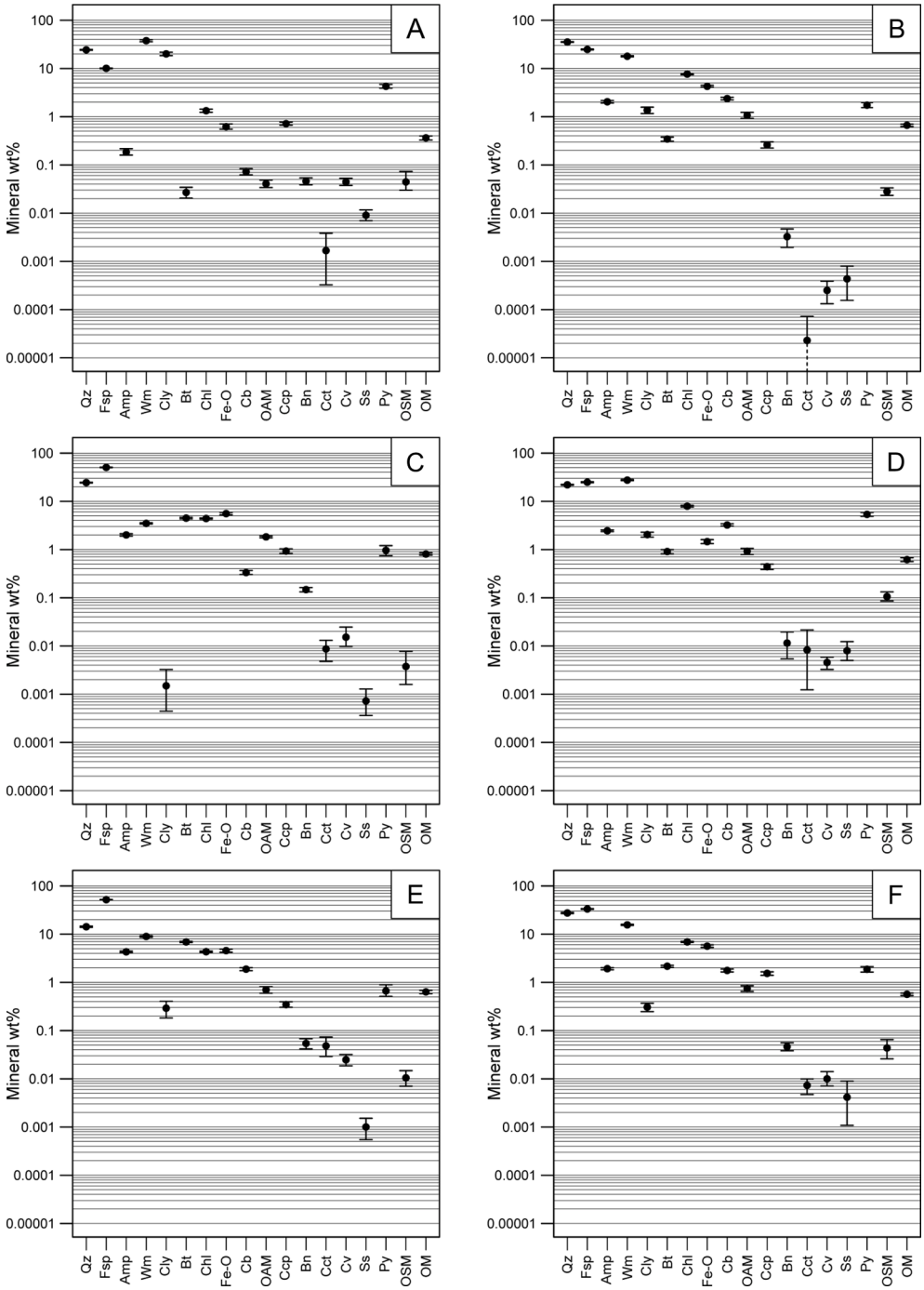

Fig. B1. Median value of bootstrapped modal mineralogy, with error bars representing 95 % confidence intervals. (A) TRSD013 64–104 m; (B) TRSD013 356–396 m; (C) TRSD013 758–798 m; (D) TRSD017 240–280 m; (E) TRSD017 346–386 m; (F) TRSD017 386–426 m.

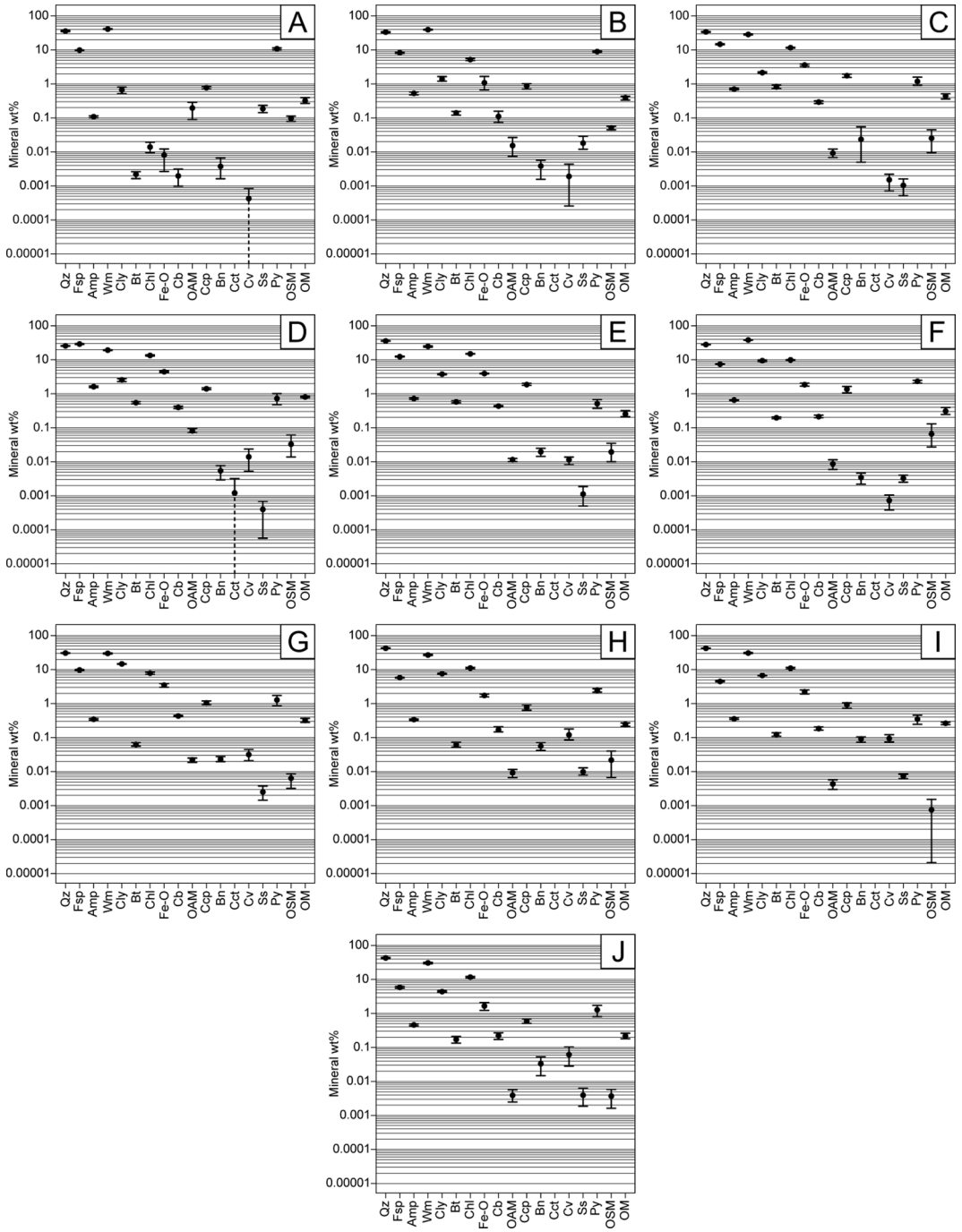

Fig. B2. Median value of bootstrapped modal mineralogy, with error bars representing 95 % confidence intervals. (A) TRSD013 152–156 m; (B) TRSD013 156–160 m; (C) TRSD013 160–164 m; (D) TRSD013 164–168 m; (E) TRSD013 168–172 m; (F) TRSD013 172–176 m; (G) TRSD013 176–180 m; (H) TRSD013 180–184 m; (I) TRSD013 184–188 m; (J) TRSD013 188–192 m.

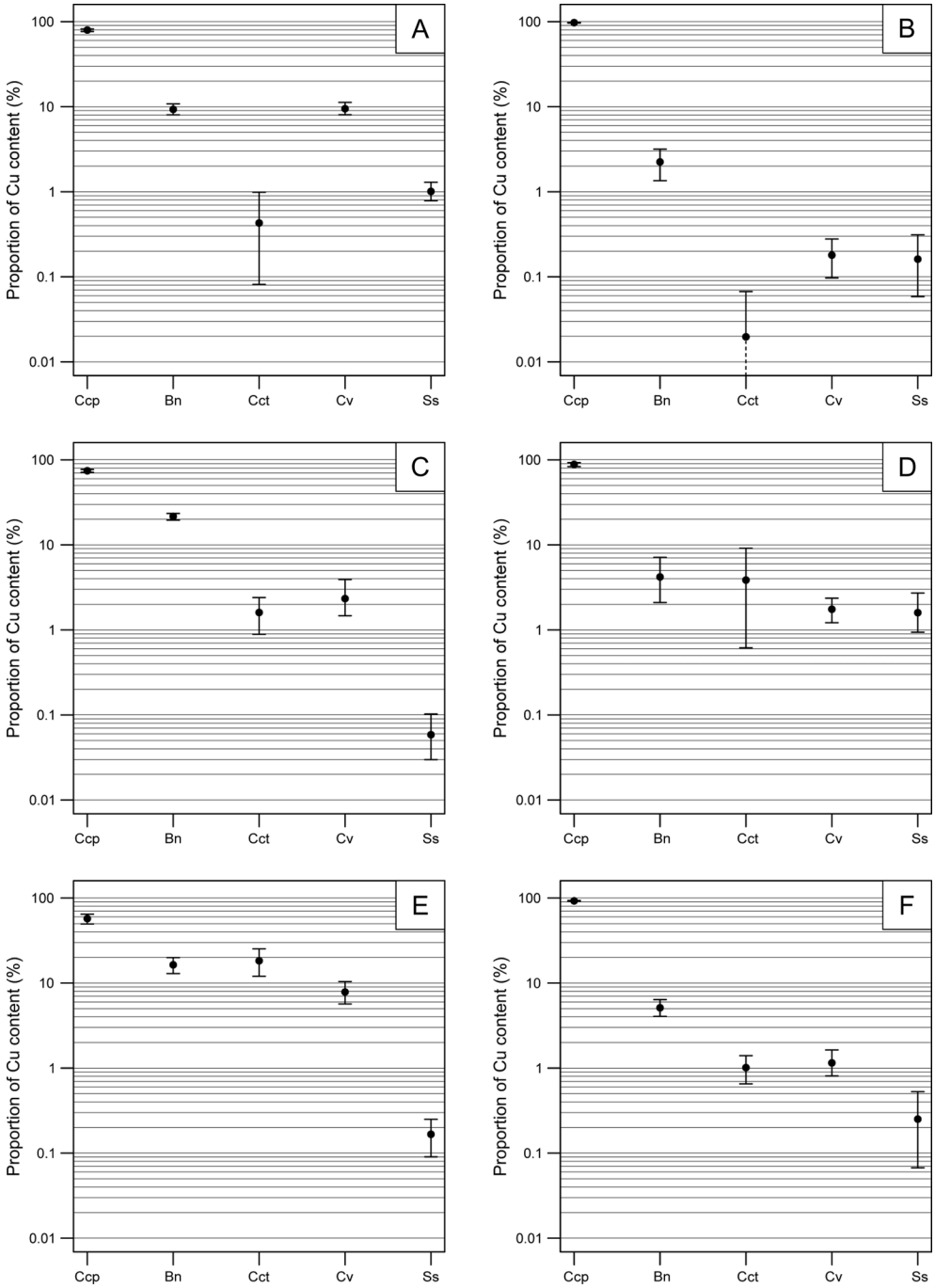

Fig. B3. Median value of bootstrapped copper deportment, with error bars representing 95 % confidence intervals. (A) TRSD013 64–104 m; (B) TRSD013 356–396 m; (C) TRSD013 758–798 m; (D) TRSD017 240–280 m; (E) TRSD017 346–386 m; (F) TRSD017 386–426 m.

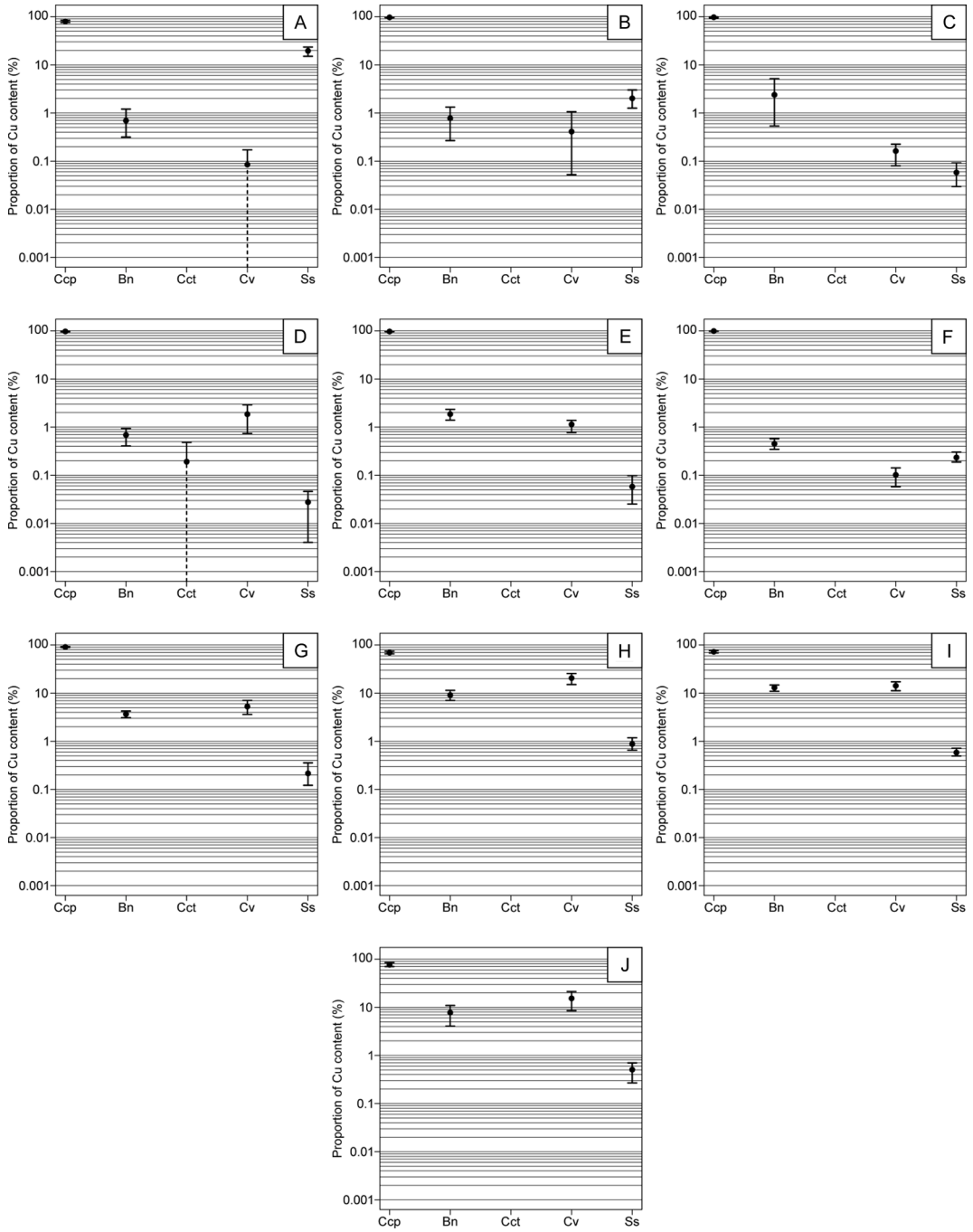

Fig. B4. Median value of bootstrapped copper deportment, with error bars representing 95 % confidence intervals. (A) TRSD013 152–156 m; (B) TRSD013 156–160 m; (C) TRSD013 160–164 m; (D) TRSD013 164–168 m; (E) TRSD013 168–172 m; (F) TRSD013 172–176 m; (G) TRSD013 176–180 m; (H) TRSD013 180–184 m; (I) TRSD013 184–188 m; (J) TRSD013 188–192 m. Chalcocite was only present in sample TRSD013 164–168 m, and is therefore zero and not plotted in the other graphs.

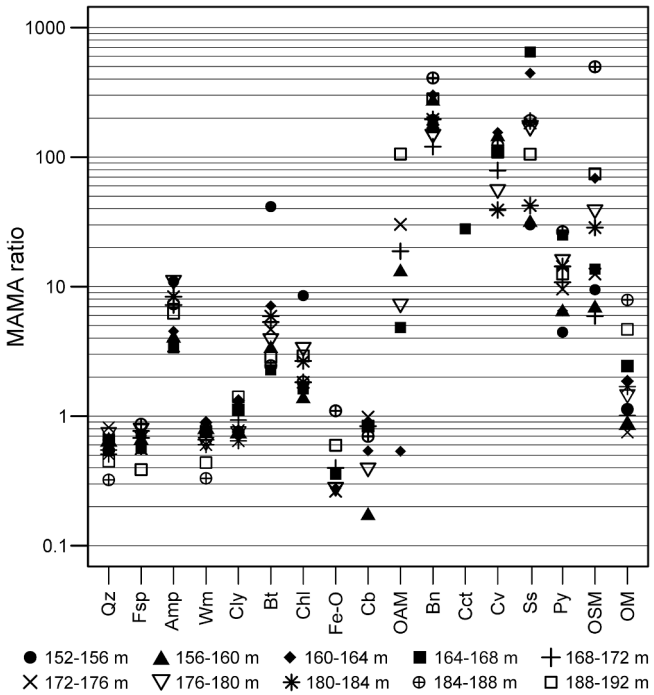

Fig. B5. Median MAMA ratio values of chalcopyrite for the 4 m interval samples, calculated from the bootstrap resampling results of chalcopyrite mineral associations and modal mineralogy.

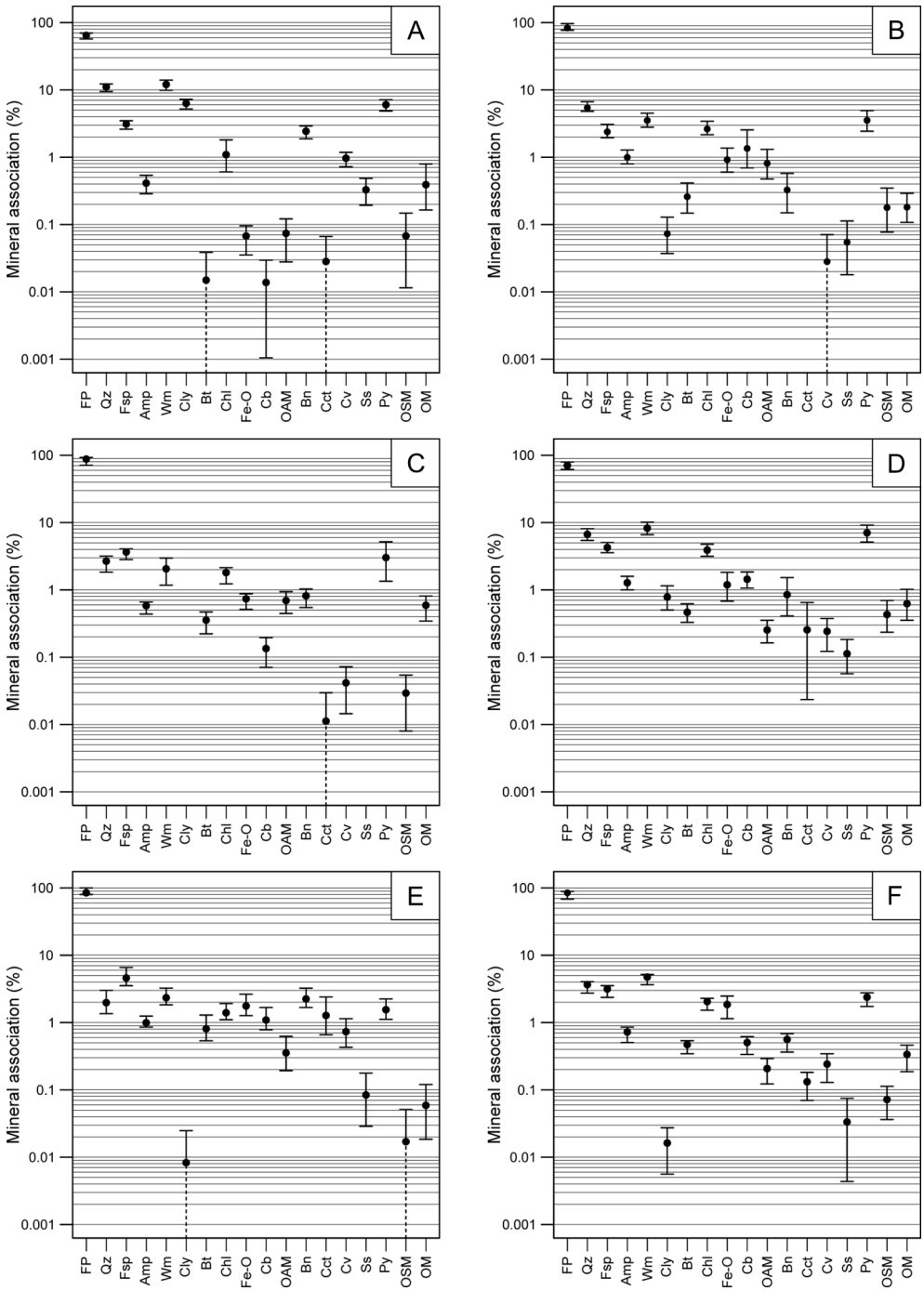

Fig. B6. Median value of bootstrapped chalcopyrite mineral associations (percentage of chalcopyrite grain perimeters), with error bars representing 95 % confidence intervals. (A) TRSD013 64–104 m; (B) TRSD013 356–396 m; (C) TRSD013 758–798 m; (D) TRSD017 240–280 m; (E) TRSD017 346–386 m; (F) TRSD017 386–426 m.

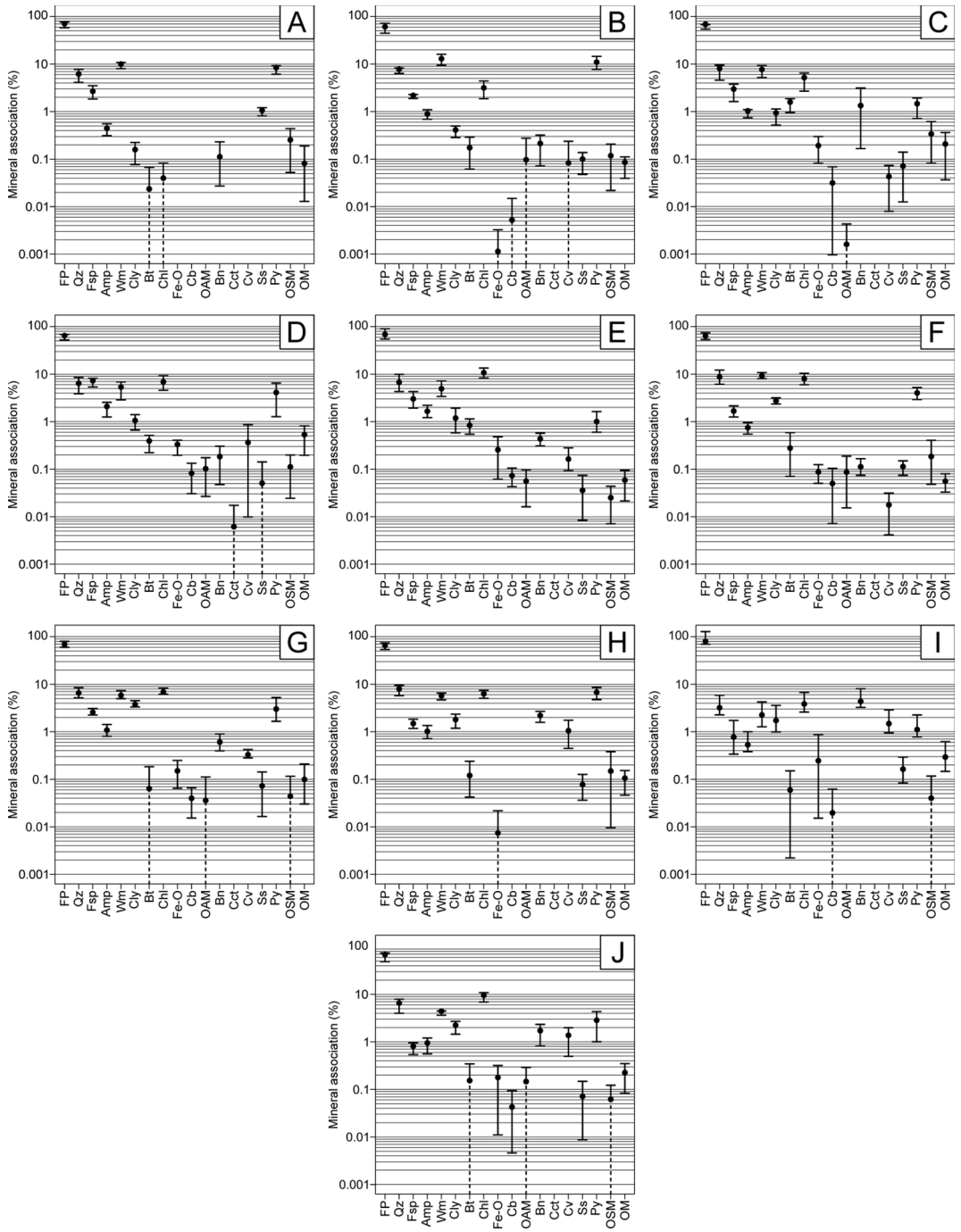

Fig. B7. Median value of bootstrapped chalcopyrite mineral associations (percentage of chalcopyrite grain perimeters), with error bars representing 95 % confidence intervals. The dashed lines in A, B, C, D, G, H, I and J symbolise that the 2.5th percentile of the particular mineral was 0. (A) TRSD013 152–156 m; (B) TRSD013 156–160 m; (C) TRSD013 160–164 m; (D) TRSD013 164–168 m; (E) TRSD013 168–172 m; (F) TRSD013 172–176 m; (G) TRSD013 176–180 m; (H) TRSD013 180–184 m; (I) TRSD013 184–188 m; (J) TRSD013 188–192 m.

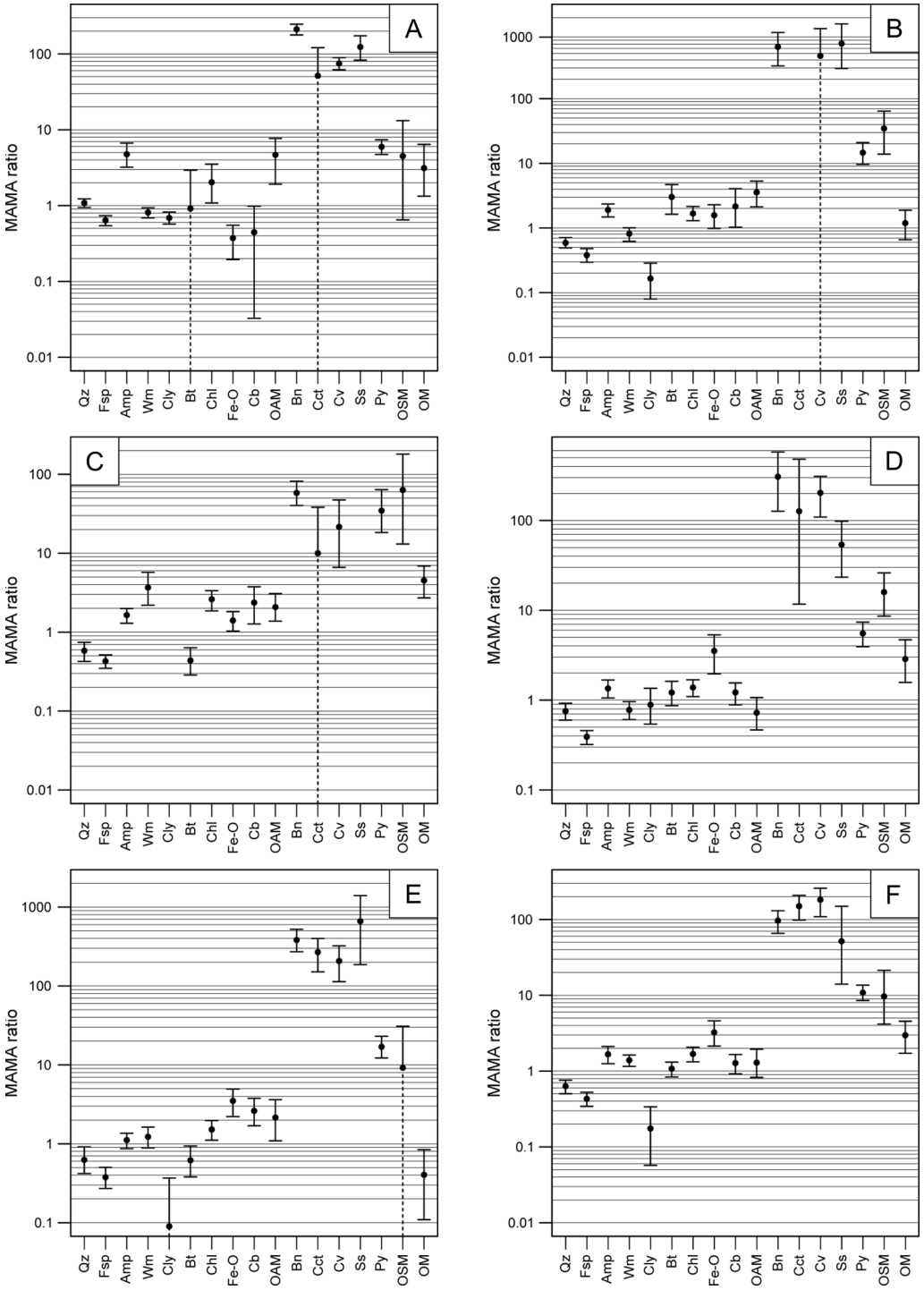

Fig. B8. Median chalcopyrite MAMA ratio values, calculated from bootstrap resampled mineral associations and mineral areas, with error bars representing 95 % confidence intervals. (A) TRSD013 64–104 m; (B) TRSD013 356–396 m; (C) TRSD013 758–798 m; (D) TRSD017 240–280 m; (E) TRSD017 346–386 m; (F) TRSD017 386–426 m.

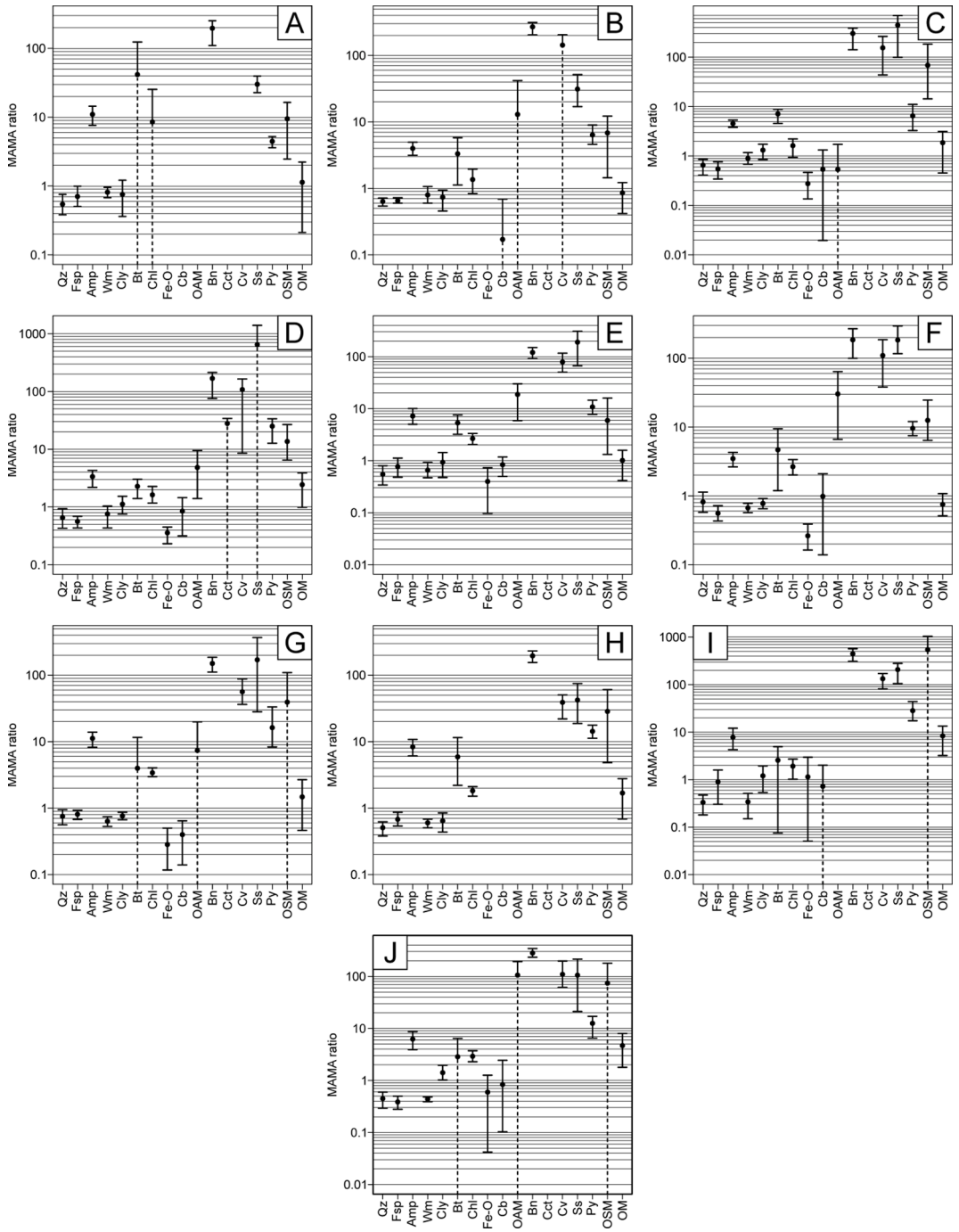

Fig. B9. Median chalcopyrite MAMA ratio values, calculated from bootstrap resampled mineral associations and mineral areas, with error bars representing 95 % confidence intervals. (A) TRSD013 152–156 m; (B) TRSD013 156–160 m; (C) TRSD013 160–164 m; (D) TRSD013 164–168 m; (E) TRSD013 168–172 m; (F) TRSD013 172–176 m; (G) TRSD013 176–180 m; (H) TRSD013 180–184 m; (I) TRSD013 184–188 m; (J) TRSD013 188–192 m.

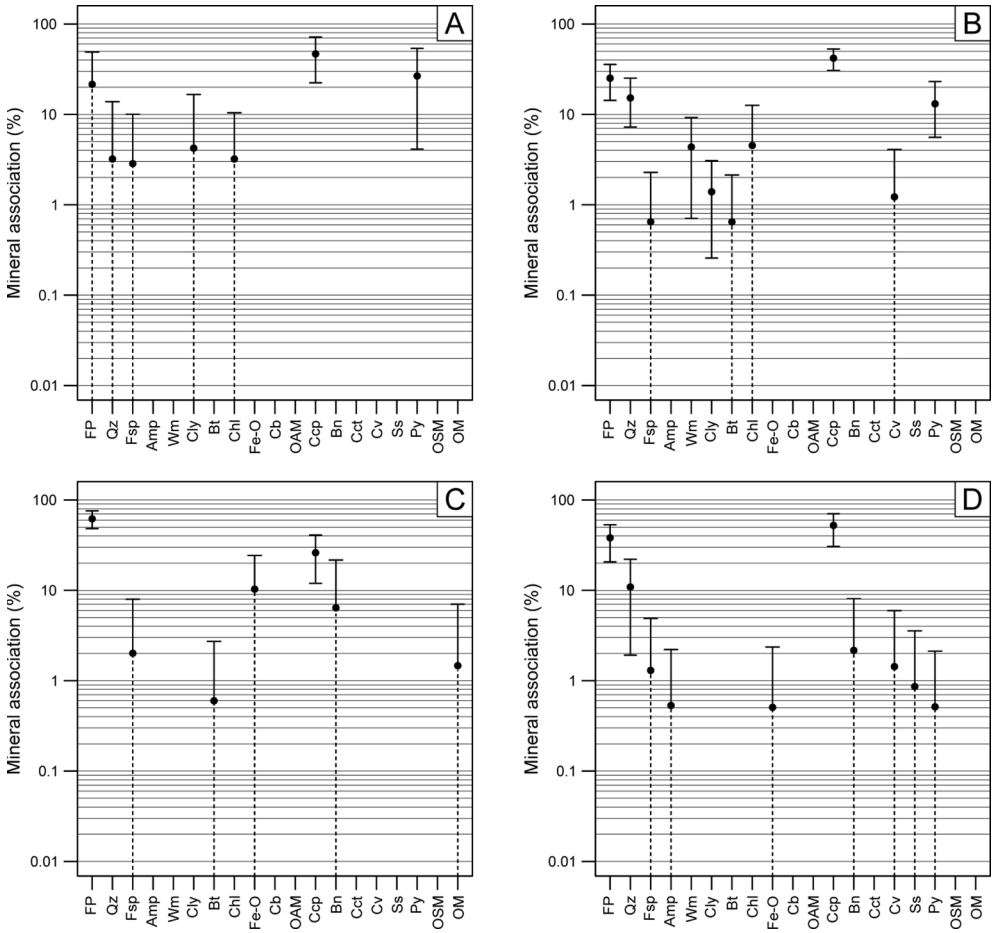

Fig. B10. Median value of bootstrapped gold mineral associations (percentage of chalcopyrite grain perimeters), with error bars representing 95 % confidence intervals. (A) TRSD013 64–104 m; (B) TRSD013 152–192 m, including gold grains from both the 40 m and 4 m samples; (C) TRSD013 758–798 m; (D) TRSD017 386–426 m.

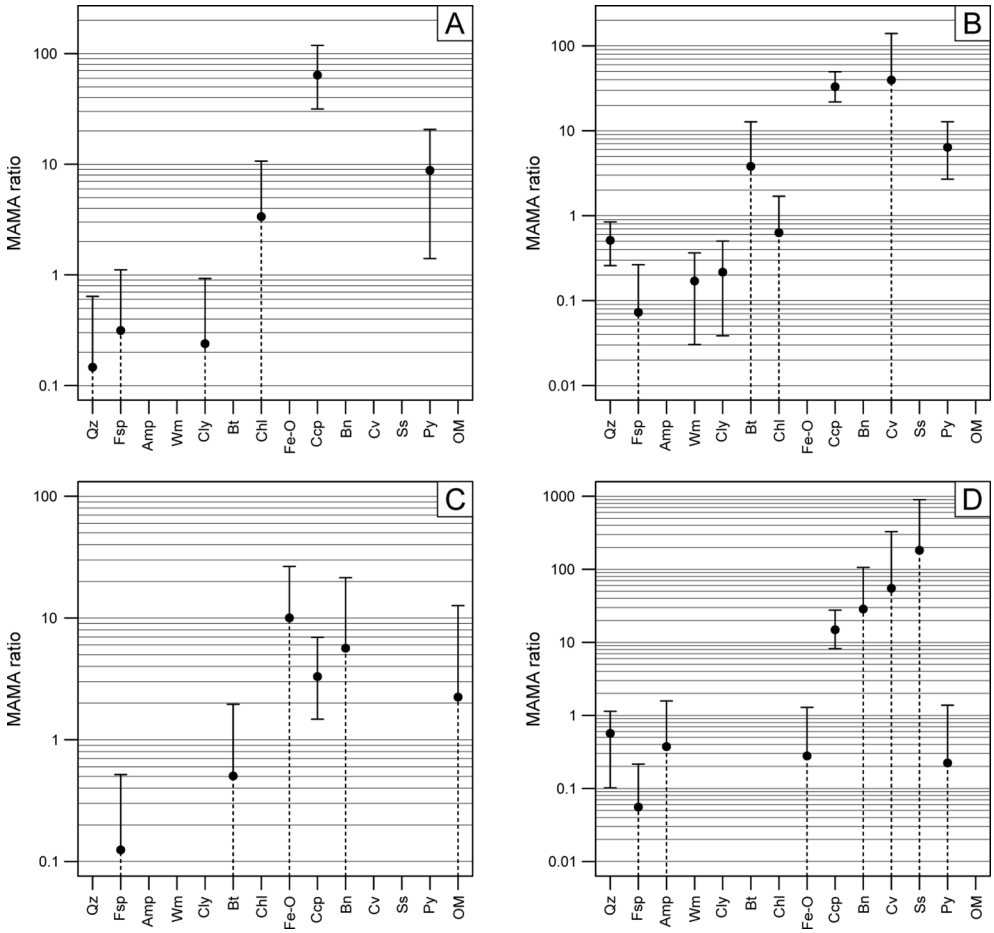

Fig. B11. Median gold MAMA ratio values, calculated from bootstrap resampled mineral associations and mineral areas, with error bars representing 95 % confidence intervals. (A) TRSD013 64–104 m; (B) TRSD013 152–192 m, including gold grains from both the 40 m and 4 m samples; (C) TRSD013 758–798 m; (D) TRSD017 386–426 m.

Appendix C

See Fig. C1 and Fig. C2
See Table C1 and Table C2

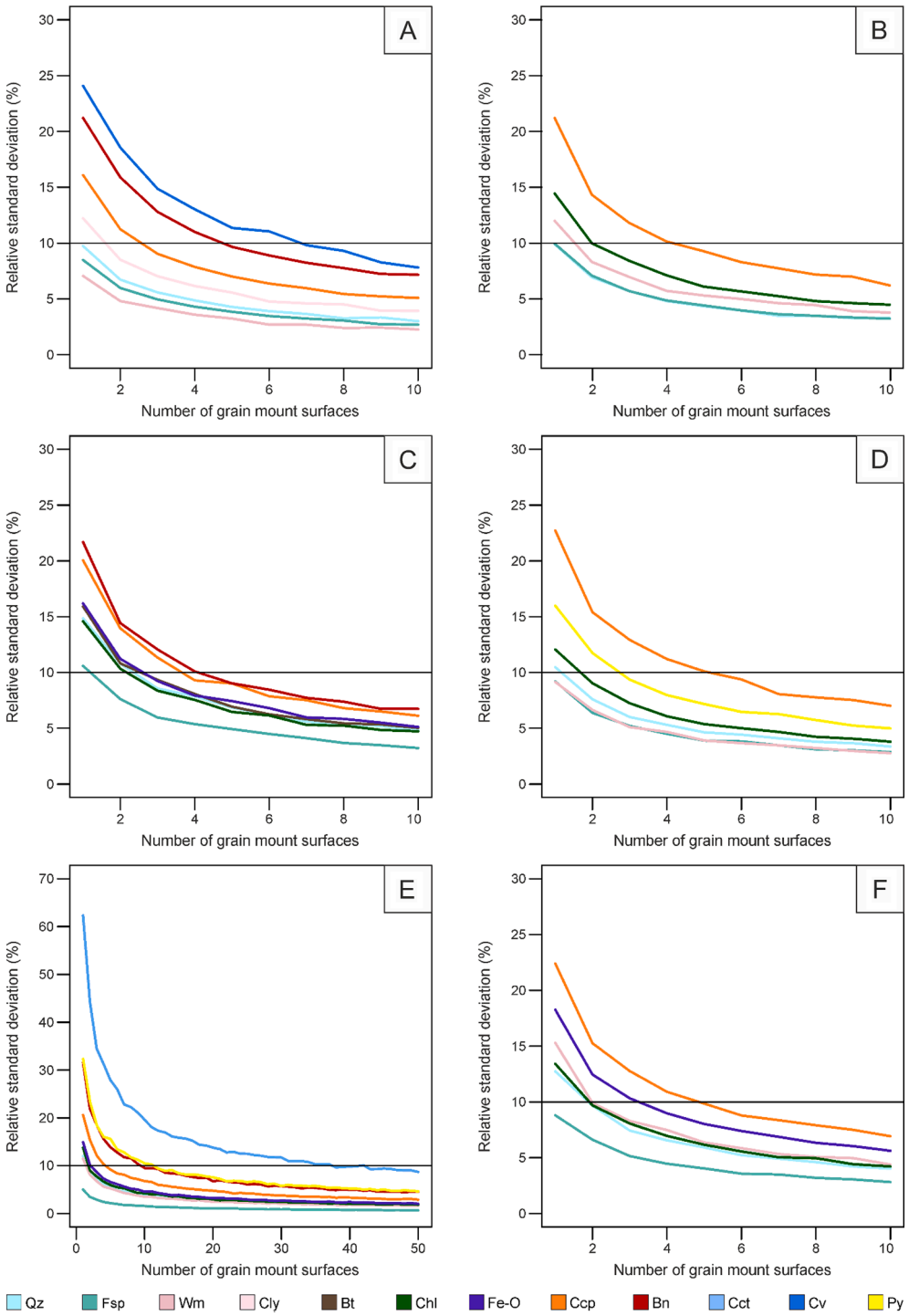

Fig. C1. Bootstrap resampling of modal mineralogy of the 40 m intervals for minerals with an abundance of > 5 wt%, or Cu-bearing minerals which contribute > 5 % of Cu deportment. ***N*** was increased until the required *RSD* of 10 % was reached for all minerals. (A) TRSD013 64–104 m; (B) TRSD013 356–396 m; (C) TRSD013 758–798 m; (D) TRSD017 240–280 m; (E) TRSD017 346–386 m; (F) TRSD017 386–426 m.

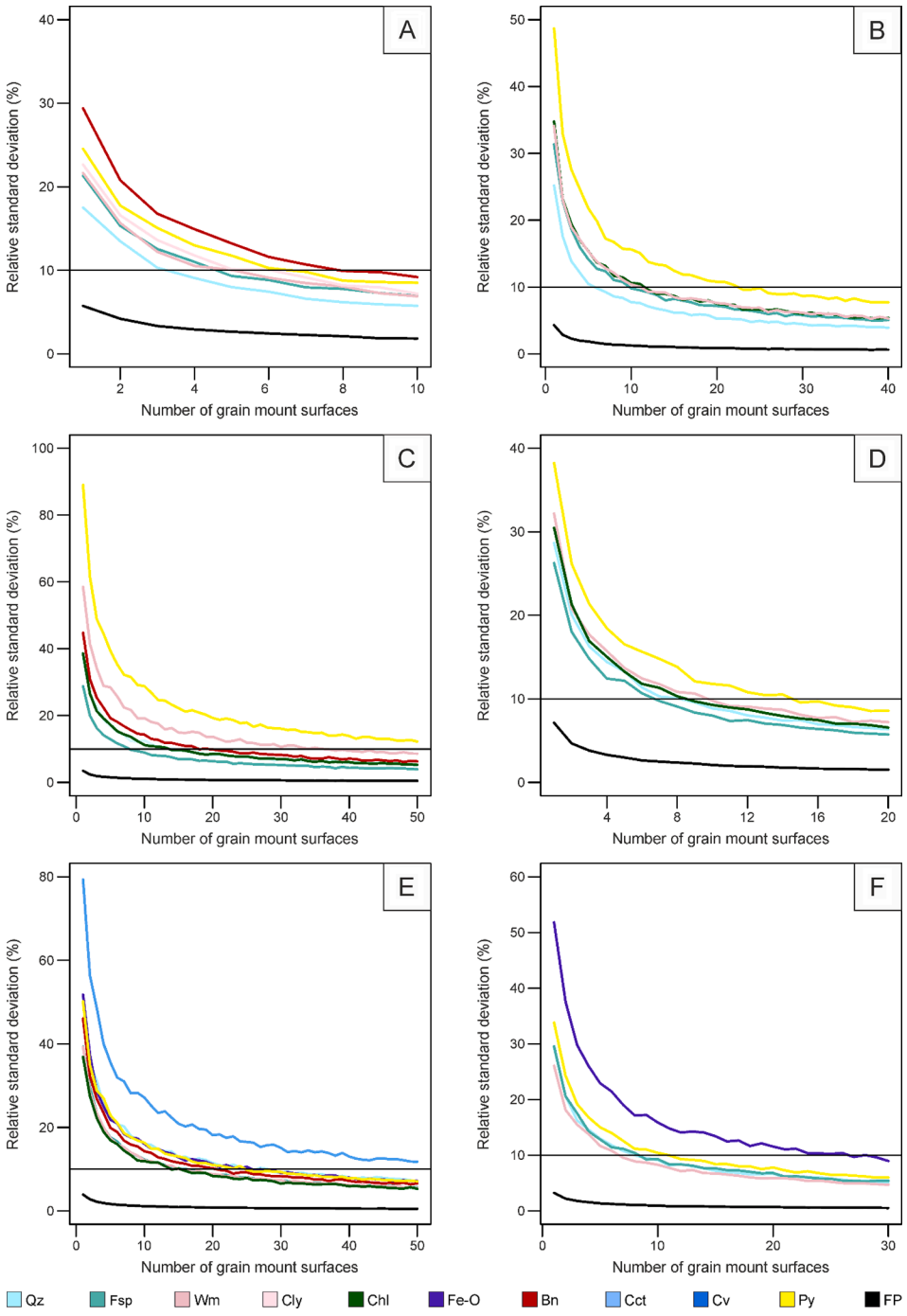

Fig. C2. Bootstrap resampling of mineral associations of chalcopyrite in the 40 m intervals for minerals with an association of > 5 % when free perimeter is excluded. ***N*** was increased until the required *RSD* of 10 % was reached for all minerals, or to a limit of 50 surfaces. (A) TRSD013 64–104 m; (B) TRSD013 356–396 m; (C) TRSD013 758–798 m; (D) TRSD017 240–280 m; (E) TRSD017 346–386 m; (F) TRSD017 386–426 m.

Table C1
Number of grain mount surfaces necessary to reach a *RSD* of 10 % for minerals with an abundance of > 5 wt%, or Cu-bearing minerals which contribute > 5 % of Cu deportment in the 40 m interval crushed material samples. ***N*** was increased in increments of 5, to represent a whole grain mount surface composed of 5 strips, for the bootstrap resampling until the required *RSD* was reached.

Mineral	TRSD013				TRSD017		
	64–104 m	152–192 m	356–396 m	758–798 m	240–280 m	346–386 m	386–426 m
Quartz	1	1	1	2	2	2	2
Feldspars	1	1	1	1	1	1	1
White micas	1	1	3	–	1	2	3
Clay minerals	2	8	–	–	–	–	–
Biotite	–	–	–	3	–	2	–
Chlorite	–	3	2	3	2	2	2
Fe-oxides	–	–	–	3	–	3	4
Chalcopyrite	3	3	5	4	6	5	5
Bornite	5	–	–	6	–	10	–
Chalcocite	–	–	–	–	–	38	–
Covellite	7	–	–	–	–	–	–
Pyrite	–	–	–	–	3	–	–

Table C2
Number of grain mount surfaces necessary to reach a *RSD* of 10 % for the mineral associations of chalcopyrite, with minerals with an association of > 5 % when free perimeter is excluded, in the 40 m interval crushed material samples. ***N*** was increased in increments of 5, to represent a whole grain mount surface composed of 5 strips, for the bootstrap resampling until the required *RSD* was reached, or until the number of surfaces reached 50.

Mineral	TRSD013				TRSD017		
	64–104 m	152–192 m	356–396 m	758–798 m	240–280 m	346–386 m	386–426 m
Quartz	4	4	7	15	9	29	8
Feldspars	5	6	11	8	7	17	9
White micas	6	5	12	37	10	16	7
Clay minerals	7	6	–	–	–	–	–
Chlorite	–	6	13	14	9	14	–
Fe-oxides	–	–	–	–	–	26	26
Bornite	8	–	–	20	–	21	–
Chalcocite	–	–	–	–	–	> 50	–
Pyrite	7	7	24	> 50	15	25	12
Free perimeter	1	1	1	1	1	1	1
Chalcopyrite content (wt%)	0.7	0.9	0.3	0.9	0.4	0.4	1.5

References

Arif, J., Baker, T., 2004. Gold paragenesis and chemistry at Batu Hijau, Indoneisa: Implications for gold-rich porphyry copper deposits. Miner. Depos. 39, 523–535. https://doi.org/10.1007/s00126-004-0433-0.

Bachmann, K., Frenzel, M., Krause, J., Gutzmer, J., 2017. Advanced Identification and Quantification of In-Bearing Minerals by Scanning Electron Microscope-Based Image Analysis. Microsc. Microanal. 23, 527–537. https://doi.org/10.1017/S1431927617000460.

Bachmann, K., Osbahr, I., Tolosana-Delgado, R., Chetty, D., Gutzmer, J., 2018. Variation in Platinum Group Mineral and Base Metal Sulfide Assemblages in the Lower Group Chromitites of the Western Bushveld Complex, South Africa. Can. Mineral. 56, 723–743. https://doi.org/10.3749/canmin.1700094.

Baker, T., 2019. Gold ± copper endowment and deposit diversity in the western Tethyan Magmatic Belt, Southeast Europe: Implications for exploration. Econ. Geol. 114, 1237–1250. https://doi.org/10.5382/econgeo.4643.

Benvie, Byron, Chapman, Nicole M., Robinson, David J., Kuhar, Laura L., 2013. A robust statistical method for mineralogical analysis in geometallurgical diagnostic leaching. Miner. Eng. 52, 178–183. https://doi.org/10.1016/j.mineng.2013.06.010.

Berbeleac, I., Udubaşa, S.S., Iatan, E.-L., Vişan, M., 2014. Geological and Structural Constraints on the Localization of Neogene Porphyry– Epithermal Related Cu-Au (Mo), and Epigenetic Hydrothermal Deposits/Prospects from South Apuseni Mts. Romania. Rom. J. Miner. Depos. 87, 47–52.

Blannin, R., Tusa, L., Birtel, S., Gutzmer, J., Gilbricht, S., Ivăşcanu, P., 2019. Metal deportment and ore variability of the Bolcana porphyry Au – Cu system (Apuseni Mts , Romania) – Implications for ore processing. 15th SGA Bienn. Meet. 2019 Proc.

Buchmann, M., Schach, E., Tolosana-Delgado, R., Leißner, T., Astoveza, J., Kern, M., Möckel, R., Ebert, D., Rudolph, M., van den Boogaart, K.G., Peuker, U.A., 2018. Evaluation of magnetic separation efficiency on a cassiterite-bearing skarn ore by means of integrative SEM-based image and XRF–XRD data analysis. Minerals 8. https://doi.org/10.3390/min8090390.

Butcher, A.R., Helms, T.A., Gottlieb, P., Bateman, R., Ellis, S., Johnson, N.W., 2000. Advances in the quantification of gold deportment by QemSCAN. Seventh Mill Oper. Conf. Kalgoorlie, WA, AusIMM 267–271.

Cardon, O., Reisberg, L., André-Mayer, A.S., Leroy, J.L., Milu, V., Zimmermann, C., 2008. Re-Os systematics of pyrite from the bolcana porphyry copper deposit, Apuseni Mountains. Romania. Econ. Geol. 103, 1695–1702. https://doi.org/10.2113/gsecongeo.103.8.1695.

Chayes, F., 1945. Petrographic analysis by fragment counting: Part 2. Precision of micro-sampling and the combination error of sampling and counting. Econ. Geol. 40, 517–525. https://doi.org/10.2113/gsecongeo.40.8.517.

Chayes, F., 1944. Petrographic analysis by fragment counting: Part 1. The Counting Error. Econ. Geol. 39, 484–505. https://doi.org/10.2113/gsecongeo.39.7.484.

Chernick, M.R., 1999. Bootstrap Methods: A Practitioner's Guide. Wiley, New York.

Cioacă, M.E., 2013. Investigation of the rare elements from the porphyry copper deposits in Romania.

Cioacă, M.E., Munteanu, M., Qi, L., Costin, G., 2014. Trace element concentrations in porphyry copper deposits from Metaliferi Mountains, Romania: A reconnaissance study. Ore Geol. Rev. 63, 22–39. https://doi.org/10.1016/j.oregeorev.2014.04.016.

Clark, I., 2010. Statistics or geostatistics? Sampling error or nugget effect? J. South. African Inst. Min. Metall. 110, 307–312.

Core, D.P., Kesler, S.E., Essene, E.J., 2006. Unusually Cu-rich magmas associated with giant porphyry copper deposits: Evidence from Bingham, Utah. Geology 34, 41–44.

Cropp, A.F., Goodall, W.R., Bradshaw, D.J., 2013. The Influence of Textural Variation and Gangue Mineralogy on Recovery of Copper by Flotation from Porphyry Ore – A Review. Second AusIMM Int. Geometallurgy Conf. 30, 279–291.

Dénes, Réka, Kiss, Gabriella B., Ivăşcanu, Paul, 2015. Petrographic and geochemical study of the porphyry and epithermal mineralization in the bolcana magmatic-hydrothermal system (Apuseni Mts, Romania). 13th SGA Bienn. Meet. 2015 Proc.

Dominy, S.C., Edgar, W.B., 2012. Approaches to reporting grade uncertainty in high nugget gold veins. Trans. Institutions Min. Metall. Sect. B Appl. Earth Sci. 121, 29–42. https://doi.org/10.1179/1743275812Y.0000000013.

Dominy, S.C., Johansen, G.F., Annels, A.E., 2001. Bulk sampling as a tool for the grade evaluation of gold-quartz reefs. Appl. Earth Sci. Trans. Institutions Min. Metall. Sect. B 110, B176–B191. https://doi.org/10.1179/aes.2001.110.3.176.

Dominy, S.C., O'Connor, L., Glass, H.J., Purevgerel, S., Xie, Y., 2018. Towards representative metallurgical sampling and gold recovery testwork programmes. Minerals 8. https://doi.org/10.3390/min8050193.

Dominy, S.C., Platten, I.M., Raine, M.D., 2003. Grade and geological continuity in high-nugget effect gold-quartz reefs: Implications for resource estimation and reporting. Appl. Earth Sci. Trans. Inst. Min. Metall. Sect. B 112, B239–B259. https://doi.org/10.1179/037174503225003116.

Efron, B., 1979. Bootstrap methods: another look at the jacknife. Ann. Stat. 7, 1–26.

Evans, C.L., Napier-Munn, T.J., 2013. Estimating error in measurements of mineral grain size distribution. Miner. Eng. 52, 198–203. https://doi.org/10.1016/j.mineng.2013.09.005.

Fandrich, R., Gu, Y., Burrows, D., Moeller, K., 2007. Modern SEM-based mineral liberation analysis. Int. J. Miner. Process. 84, 310–320. https://doi.org/10.1016/j.minpro.2006.07.018.

Frenzel, M., Bachmann, K., Carvalho, J.R.S., Relvas, J.M.R.S., Pacheco, N., Gutzmer, J., 2018. The geometallurgical assessment of by-products—geochemical proxies for the complex mineralogical deportment of indium at Neves-Corvo, Portugal. Miner. Depos. https://doi.org/10.1007/s00126-018-0849-6.

Goodall, W.R., 2008. Characterisation of mineralogy and gold deportment for complex tailings deposits using QEMSCAN®. Miner. Eng. 21, 518–523. https://doi.org/10.1016/j.mineng.2008.02.022.

Goodall, W.R., Butcher, A.R., 2012. The use of QEMSCAN in practical gold deportment studies. Trans. Institutions Min. Metall. Sect. C Miner. Process. Extr. Metall. 121, 199–204. https://doi.org/10.1179/1743285512Y.0000000021.

Gottlieb, P., Wilkie, G., Sutherland, D., Ho-Tun, E., Suthers, S., Perera, K., Jenkins, B., Spencer, S., Butcher, A., Rayner, J., 2000. Using quantitative electron microscopy for process mineralogy applications. Jom 52, 24–25. https://doi.org/10.1007/s11837-000-0126-9.

Gregory, M.J., Lang, J.R., Gilbert, S., Hoal, K.O., 2013. Geometallurgy of the Pebble porphyry copper-gold-molybdenum deposit, Alaska: Implications for gold distribution and paragenesis. Econ. Geol. 108, 463–482. https://doi.org/10.2113/econgeo.108.3.463.

Gu, Y., 2003. Automated Scanning Electron Microscope Based Mineral Liberation Analysis, An Introduction to JKMRC/FEI Mineral Liberation Analyser. J. Miner. Mater. Charact. Eng. 02, 33–41. https://doi.org/10.4236/jmmce.2003.21003.

Guseva, O., Opitz, A.K.B., Broadhurst, J.L., Harrison, S.T.L., Becker, M., 2021. Characterisation and prediction of acid rock drainage potential in waste rock: Value of integrating quantitative mineralogical and textural measurements. Miner. Eng. 163, 106750 https://doi.org/10.1016/j.mineng.2020.106750.

Gy, P., 1982. Sampling of Particulate Materials: Theory and Practice. Elsevier Scientific Publ. Co., Amsterdam, New York.

Hannula, J., Kern, M., Luukkanen, S., Roine, A., van den Boogaart, K.G., Reuter, M.A., 2018. Property-based modelling and simulation of mechanical separation processes using dynamic binning and neural networks. Miner. Eng. 126, 52–63. https://doi.org/10.1016/j.mineng.2018.06.017.

Heinig, T., Bachmann, K., Boogaart, G. Van Den, Gutzmer, J., 2015. Monitoring gravitational and particle shape settling effects on MLA sampling preparation. IAMG Conf. 2015, Freiberg, Ger.

Ivăşcanu, P., Baker, T., Lewis, P., Kulcsar, Z., Dénes, R., Tamas, C., 2019. Bolcana, Romania: Geology and discovery history of a gold rich porphyry deposit, in: NewGenGold 2019 Conference Proceedings: Perth, Australia, 2019. pp. 69–82.

Ivăşcanu, P., Kulcsar, Z., Dénes, R., Baker, T., Lewis, P., 2018. Bolcana Porphyry Au-Cu Deposit, Apuseni Mountains, Romania. AME Roundup 2018 Core Shack Abstr. Guid. 31.

Kern, M., Kästner, J., Tolosana-Delgado, R., Jeske, T., Gutzmer, J., 2019. The inherent link between ore formation and geometallurgy as documented by complex tin mineralization at the Hämmerlein deposit (Erzgebirge, Germany). Miner. Depos. 54, 683–698. https://doi.org/10.1007/s00126-018-0832-2.

Kern, M., Möckel, R., Krause, J., Teichmann, J., Gutzmer, J., 2018. Calculating the deportment of a fine-grained and compositionally complex Sn skarn with a modified approach for automated mineralogy. Miner. Eng. 116, 213–225. https://doi.org/10.1016/j.mineng.2017.06.006.

Kesler, S.E., Chryssoulis, S.L., Simon, G., 2002. Gold in porphyry copper deposits: Its abundance and fate. Ore Geol. Rev. 21, 103–124. https://doi.org/10.1016/S0169-1368(02)00084-7.

Lastra, R., Paktunc, D., 2016. An estimation of the variability in automated quantitative mineralogy measurements through inter-laboratory testing. Miner. Eng. https://doi.org/10.1016/j.mineng.2016.06.025.

Lavrent'ev, Y.G., Karmanov, N.S., Usova, L. V., 2015. Electron probe microanalysis of minerals: Microanalyzer or scanning electron microscope? Russ. Geol. Geophys. 56, 1154–1161. https://doi.org/10.1016/j.rgg.2015.07.006.

Leichliter, S.E., 2013. Gold Deportment and Geometallurgical Recovery Model for the La Colosa, Porphyry Gold Deposit. University of Tasmania, Colombia.

Leigh, G.M., Sutherland, D.N., Gottlieb, P., 1993. Confidence limits for liberation measurements. Miner. Eng. 6, 155–161. https://doi.org/10.1016/0892-6875(93)90129-B.

Leißner, T., Bachmann, K., Gutzmer, J., Peuker, U.A., 2016. MLA-based partition curves for magnetic separation. Miner. Eng. 94, 94–103. https://doi.org/10.1016/j.mineng.2016.05.015.

Mariano, R.A., Evans, C.L., 2015. Error analysis in ore particle composition distribution measurements. Miner. Eng. 82, 36–44. https://doi.org/10.1016/j.mineng.2015.06.001.

Milu, V., Leroy, J.L., Piantone, P., 2003. The Bolcana Cu-Au ore deposit (Metalifero Mountains, Romania): first data on the alteration and related mineralisation. Comptes Rendus - Geosci. 335, 671–680. https://doi.org/10.1016/S1631-0713(03)00120-2.

Osbahr, I., Krause, J., Bachmann, K., Gutzmer, J., 2015. Efficient and Accurate Identification of Platinum-Group Minerals by a Combination of Mineral Liberation and Electron Probe Microanalysis with a New Approach to the Offline Overlap Correction of Platinum-Group Element Concentrations. Microsc. Microanal. 21, 1080–1095. https://doi.org/10.1017/S1431927615000719.

Parian, M., Lamberg, P., Möckel, R., Rosenkranz, J., 2015. Analysis of mineral grades for geometallurgy: Combined element-to-mineral conversion and quantitative X-ray diffraction. Miner. Eng. 82, 25–35. https://doi.org/10.1016/J.MINENG.2015.04.023.

Reed, S.J.B., 2005. Electron Microprobe Analysis and Scanning Electron Microscopy in Geology, Cambridge University Press. https://doi.org/https://doi.org/10.1017/CBO9780511610561.

Schach, E., Buchmann, M., Tolosana-Delgado, R., Leißner, T., Kern, M., van den Boogaart, G., Rudolph, M., Peuker, U.A., 2019. Multidimensional characterization of separation processes – Part 1: Introducing kernel methods and entropy in the context of mineral processing using SEM-based image analysis. Miner. Eng. 137, 78–86. https://doi.org/10.1016/j.mineng.2019.03.026.

Schulz, B., Sandmann, D., Gilbricht, S., 2020. Sem-based automated mineralogy and its application in geo-and material sciences. Minerals 10, 1–26. https://doi.org/10.3390/min10111004.

Sillitoe, R.H., 2010. Porphyry copper systems. Econ. Geol. 105, 3–41. https://doi.org/10.2113/gsecongeo.105.1.3.

Simon, G., Kesler, S.E., Essene, E.J., Chryssoulis, S.L., 2000. Gold in porphyry copper deposits: Experimental determination of the distribution of gold in the Cu-Fe-S system at 400 degrees to 700 degrees C. Econ. Geol. 95, 259–270.

Van der Plas, L., Tobi, A., 1965. A chart for judging the reliability of point counting results. Am. J. Sci. 263, 87–90.

Warlo, M., Wanhainen, C., Bark, G., Butcher, A.R., McElroy, I., Brising, D., Rollinson, G. K., 2019. Automated Quantitative Mineralogy Optimized for Simultaneous Detection of (Precious/Critical) Rare Metals and Base Metals in A Production-Focused Environment. Minerals 9, 440. https://doi.org/10.3390/min9070440.

Whitney, D.L., Evans, B.W., 2010. Abbreviations for names of rock-forming minerals. Am. Mineral. 95, 185–187. https://doi.org/10.2138/am.2010.3371.

Zhou, J., Mermillod-Blondin, R., Cousin, P., 2009. Deportment of Gold and Silver in the Pinos Altos Composite and Leach Residues: Implications for Recovery Improvement. World Gold Conf. 2009, South. African Inst. Min. Metall. 75–83.